HHS Public Access

Author manuscript

Nat Neurosci. Author manuscript; available in PMC 2020 April 21.

Published in final edited form as:

Nat Neurosci. 2019 November ; 22(11): 1782–1792. doi:10.1038/s41593-019-0514-0.

Noradrenergic signaling the wakeful state inhibits microglial surveillance and synaptic plasticity in the mouse visual cortex.

Rianne D. Stowell[1,2,†], **Grayson O. Sipe**[3,†], **Ryan P. Dawes**[1,2], **Hanna N. Batchelor**[1], **Katheryn A. Lordy**[1], **Brendan S. Whitelaw**[1,2], **Mark B. Stoessel**[1,2], **Jean M. Bidlack**[4], **Edward Brown**[5], **Mriganka Sur**[3], **Ania K. Majewska**[1,6,*]

[1]Department of Neuroscience, University of Rochester Medical Center, Rochester, NY, USA.

[2]Neuroscience Graduate Program, University of Rochester Medical Center, Rochester, NY, USA.

[3]Picower Institute for Learning and Memory, Department of Brain and Cognitive Sciences, Massachusetts Institute of Technology, Cambridge, MA, USA.

[4]Department of Pharmacology and Physiology, University of Rochester Medical Center, Rochester, NY, USA.

[5]Department of Biomedical Engineering, University of Rochester, Rochester, NY, USA.

[6]Center for Visual Science, University of Rochester Medical Center, Rochester, NY, USA.

Abstract

Microglia are the brain's resident innate immune cells and also have a role in synaptic plasticity. Microglial processes continuously survey the brain parenchyma, interact with synaptic elements and maintain tissue homeostasis. However, the mechanisms that control surveillance and its role in synaptic plasticity are poorly understood. Microglial dynamics in vivo have been primarily studied in anesthetized animals. Here we report that microglial surveillance and injury response are reduced in awake mice compared to anesthetized mice, suggesting that arousal state modulates microglial function. Pharmacological stimulation of β2-adrenergic receptors recapitulated these observations and disrupted experience-dependent plasticity, and these effects required the presence

[*]**Correspondence:** Ania Majewska, University of Rochester Medical Center, 601 Elmwood Avenue, Box 603, Rochester, New York 14642, (585) 275-4173, Fax: (585) 756-5334, ania_majewska@urmc.rochester.edu.

Author Contributions

R.D.S, G.O.S, and A.K.M conceived the project. R.D.S, G.O.S, R.P.D, H.N.B, K.A.L., B.S.W, and M.B.S. carried out experiments and data analysis. R.D.S carried out iOS imaging experiments and analysis in Cx3cr1CreERT/$\beta_2$fl/fl, Cx3cr1CreERT, C57BL6J mice, and all *in vivo* two-photon experiments characterizing awake v. anesthetized mice, adrenergic pharmacological agents and imaging experiments utilizing Cx3cr1CreERT/$\beta_2$fl/fl/Ai9, Cx3cr1CreERT/Ai9 mice. R.D.S also performed all FACS preparation on microglial specimens. G.O.S carried out iOS imaging experiments in C57BL6J mice and imaging experiments characterizing stress and circadian rhythms. G.O.S also performed experiments utilizing terbutaline. G.O.S performed all resonance imaging and optogenetic experiments. R.P.D carried out stress experiments. H.N.B assisted in confirmation of Cx3cr1Cre/$\beta_2$fl/fl excision and DSP4 depletion histology experiments. K.A.L carried out circadian morphology experiments. B.S.W performed all slice experiments. M.B.S. assisted with DSP4 histology experiments, and Cx3cr1Cre/$\beta_2$fl/fl expression histology. J.M.B contributed to experimental design of experiments with pharmacological agents. E.B. advised on experimental design and analysis of stress experiments. M.S. advised on experimental design and analysis of optogenetic and resonance imaging experiments. R.D.S, G.O.S, and A.K.M wrote the first draft of the manuscript. All authors contributed to the final version of the manuscript.

[†]These authors contributed equally to this work.

Competing financial interests: The authors declare no competing financial interests.

of β2-adrenergic receptors in microglia. These results indicate that microglial roles in surveillance and synaptic plasticity in the mouse brain are modulated by noradrenergic tone fluctuations between arousal states and emphasize the need to understand the effect of disruptions of adrenergic signaling in neurodevelopment and neuropathology.

Introduction

It is becoming increasingly clear that astrocytes and microglia are critical components of the "quad-partite" synapse[1]. Microglia, the innate immune cells of the central nervous system (CNS), are exquisitely sensitive to changes in brain homeostasis and rapidly alter their morphology to respond to inflammatory signals. In the absence of injury or disease, microglial arbors are highly ramified with dynamic processes that continually extend and retract through the parenchyma[2,3]. Several recent *in vivo* imaging studies have shown that these dynamics permit microglial interactions with neural elements in diverse regions of the CNS[4–7], allowing microglia to modulate synaptic remodeling and neural plasticity through the release of growth factors and enzymes or through physical synaptic contact[8–10]. While several signaling pathways, such as fractalkine, complement, and purinergic signaling, have been identified as mediating microglial function during neural circuit pruning, development, and plasticity[8,10–13], other CNS signals, such as neurotransmitters, likely also play an important role and need to be considered[14].

Recent evidence suggests that glial physiology can be dramatically altered during wakeful states. For example, astrocytic calcium signaling increases in awake mice[15]. However, studies of microglia have been performed primarily in reduced preparations or in anesthetized animals, leaving open the possibility that microglial dynamics and the resulting interactions with neurons may be altered in awake brains. In addition, evidence suggests that extracellular space may increase under sedation[16], which could greatly impact microglial surveillance, and thereby contribute to enhanced remodeling of synaptic structure[17] and increased activity-dependent plasticity[18]. Interestingly, in the non-injured brain, microglia have a high and selective expression of the β_2 adrenergic receptor (β_2-AR) relative to other CNS cell types[19,20], suggesting they may have unique responses to norepinephrine (NE), which potently modulates plasticity, learning, attention to salient stimuli, and sensory processing[17]. Furthermore, NE and β_2-ARs can impact the microglial inflammatory response[19], IL-1β production[20], and ATP-driven chemotaxis by inhibiting the P2Y12 $G\alpha_i$ signaling pathway[21]. P2Y12 is also critical for experience-dependent plasticity in the mouse adolescent visual system, and its loss impairs both the microglial response and synaptic plasticity itself[10]. Thus, NE could act through microglial β_2-ARs to modulate microglial behavior in the awake state and modulate P2Y12-dependent microglial processes that contribute to activity-dependent synaptic rearrangement.

Here, we demonstrate that microglia in the awake brain have smaller arbors, reduced parenchyma surveillance and are less responsive to injury than those in anesthetized animals, suggesting that microglial functions in awake conditions are fundamentally different than what has previously been described under anesthesia. We then recapitulate most of these changes through pharmacological stimulation or inhibition of microglial β_2-ARs. We

demonstrate that microglial β_2-ARs and cortical NE release are necessary for the morphological changes between awake and anesthetized states. Finally, we demonstrate that activation of microglial β_2-ARs impairs ocular dominance plasticity and microglial interactions with dendritic spines. Our work shows the importance of microglial β_2-AR signaling in regulating microglial surveillance of the brain, as well as the participation of these cells in experience-dependent plasticity.

Results

Anesthesia increases microglial surveillance and injury response in the cortex parenchyma

Most studies of microglial dynamics *in vivo* have been conducted in anesthetized animals or in *ex vivo* slice preparations[2,3,10,14]. However, anesthesia substantially alters numerous facets of brain physiology through diverse actions on multiple cell types. To determine whether microglial behavior is affected by anesthesia, we imaged microglial dynamics in the same adult animals when anesthetized and awake using the microglia-labeled CX3CR1^{GFP} transgenic mouse line and a chronic cranial window preparation. We found that microglia had more elaborate process arbors when mice were anesthetized with a commonly used fentanyl cocktail (also containing dexmedetomidine and midazolam) as compared to when the animals were awake (Fig. 1a–d; area under the curve (AUC); paired t-test; $p<0.001$; Maximum # of intersections paired t-test; $p<0.001$). We next examined microglial process surveillance across one hour to determine whether the decreased process ramification during wakefulness resulted in decreased parenchymal surveillance. We found a significant reduction in the total parenchymal area occupied by microglial processes in awake as compared to anesthetized states, (Fig. 1e,f; paired t-test; $p<0.01$; Supplementary Videos 1–2). It is important to note that this definition of surveillance is based on a quantitative analysis and does not address qualitative changes in microglial surveillance capabilities.

Despite the animals being habituated to head restraint before imaging, it is possible that changes in microglial morphology and surveillance in awake animals are due to factors released as a result of increased stress. To test this possibility, we imaged microglia in animals that were exposed to restraint stress prior to anesthesia and found no difference in microglial motility, morphology or surveillance (Supplementary Fig.1). We also determined that microglial morphology, surveillance or motility did not exhibit a circadian rhythmicity in anesthetized animals (Supplementary Fig.2). Based on these findings, we conclude that anesthesia produces a more complex microglial morphology and higher process coverage of the brain parenchyma.

Given the significant impact of anesthesia on microglial surveillance and morphology, we next wanted to establish if these changes could affect targeted microglial responses to acute injury. We generated focal laser ablation injuries in the cortex of the same mice while they were either awake or anesthetized, and quantified the microglial injury response of microglia in the immediate surrounding tissue over one hour (Fig. 1g; Supplementary Videos 3–4). We did not observe blood brain barrier (BBB) disruption or monocyte infiltration during this period suggesting that the GFP+ process responses were predominantly from surrounding microglia (Supplementary Fig. 3). We found that microglia had an increased response to

focal tissue injury during anesthesia as measured by the magnitude of vectors generated by the movement of microglial processes towards the injury core (Fig. 1h–j; AUC; paired t-test; $p<0.05$; Max response; paired t-test; $p=0.08$). The enhanced injury response and surveillance in anesthetized conditions suggest that wakefulness exerts a primarily inhibitory effect on microglial dynamics that is alleviated by anesthesia.

Norepinephrine release from the locus coeruleus inhibits microglial process dynamics

Anesthesia has varying effects on brain function depending on the methods and drug compositions used. Local field potential (LFP) recordings in the cortex showed that delta wave power was significantly lower in awake conditions (Fig. 1k,l), suggesting that the fentanyl cocktail puts the brain in a slow-wave dominated state. To disambiguate the sedative effects from the analgesic effects of the fentanyl cocktail on microglia, we repeated our experiments using solely dexmedetomidine (DEX), which is a known sedative that reduces NE release from the locus coeruleus (LC) and has been used to approximate natural slow-wave sleep[21]. DEX alone produced a robust increase in the size of microglial arbor (Fig. 2a–d; AUC paired t-test; $p<0.05$; Maximum # of intersections; paired t-test; $p<0.05$) and enhanced microglial surveillance (Fig. 2e,f; paired t-test; $p<0.05$; Supplementary Video 5). These effects are unlikely to be mediated by direct action of DEX on microglia, as microglial surveillance was not affected when DEX was applied to acute cortical slices (Supplementary Fig. 4). To examine the dynamics of DEX-elicited changes, we imaged microglia continuously during DEX administration and observed expansions in the microglial arbor of the same microglia after DEX (Supplementary Fig. 5a–c). DEX-elicited morphological changes were fairly rapid occurring within ~15 minutes of i.p. administration and were quickly reversible using atipamezole (Supplementary Fig. 5d–f). To explore the rapid alteration in microglial process dynamics with DEX, we used resonance two-photon imaging to capture microglial images with high temporal resolution. We found that in awake mice, fine, transient filopodia rapidly extended and retracted from the main process arbor[22]. On the other hand, pseudopodia – the bulbous endings of microglial processes where extension and retraction of terminal processes occurs - were reduced (Supplementary Fig. 5g). DEX rapidly increased the ratio of pseudopodia (Supplementary Video 6) formation relative to filopodia formation (Fig. 2g,h; paired t-test, $p<0.001$), increasing the velocity and distance traveled of terminal microglial processes (Supplementary Fig.5h–j) within ~10 minutes of administration. Thus, the effects of DEX on motility were complex, increasing the motility of terminal processes but decreasing overall motility due to the loss of motile filopodia (also observed under fentanyl anesthesia (Supplementary Fig. 6)).

To dissect the microglial mechanisms responsible for our observations, we considered signaling pathways in microglia that could affect microglial process stabilization during wakeful states. While P2Y12 and CX3CR1 did not appear to mediate these effects (Supplementary Fig. 7), NE itself is a powerful mediator of wakefulness with decreased concentrations in the cortex during anesthesia[19,23]. Additionally, the sedative effects of DEX are thought to be mediated by suppressing LC activity via auto-receptor inhibition, decreasing cortical NE release. To test whether endogenous NE release is necessary for the observed effects of DEX, we used the LC-selective neurotoxin, N-(2-chloroethyl)-N-ethyl-2-bromobenzylamine (DSP4, 2 days prior to imaging, Supplementary Figure 8), to ablate LC

axons to the cortex and compared microglial morphology in awake animals before and after DEX treatment without LC axons. We found that DSP4 treatment prevented the increased microglial arborization (Fig. 2i–k; paired t-test, $p>0.05$) and reversed the increase in surveillance previously observed with DEX treatment (Fig. 2l; paired t-test, $p<0.05$). We then asked whether optogenetic stimulation of axons locally under DEX treatment is sufficient to alter microglial process dynamics by generating a CX3CR1^{GFP}/TH-Cre mouse and bilaterally injecting flox-ChR2 in the LC. In DEX-treated animals optogenetic activation of LC axons in the cortex resulted in decreased process surveillance (Fig. 2m,n; Two-way ANOVA repeated measures ANOVA, $P<0.05$). These data suggest that LC-NE release during wakeful states reduces microglial process morphology and parenchymal surveillance.

β_2-AR agonism in anesthetized mice decreases microglial process ramification

NE exerts diverse effects on multiple cell types through a family of G-protein coupled receptors. Though it is possible that NE exerts its effects on microglia through indirect pathways involving other cell types, we focused on the direct effect on β_2-ARs because microglia are known to express β_2-ARs at higher levels than other CNS cell types in the healthy brain[20]. In addition, previous *in vitro* work has demonstrated that microglial β_2-AR signaling can inhibit chemotaxis towards ATP[24]. To test whether β_2-AR signaling alters microglial dynamics *in vivo*, we systemically applied the BBB-permeant, β_2-AR selective agonist, clenbuterol in fentanyl-anesthetized mice. To account for indirect clenbuterol effects through the periphery, mice were pre-dosed with the BBB impermeant, non-selective β-antagonist, nadolol at least one hour prior to clenbuterol dosing. Clenbuterol treatment caused a significant and sustained retraction of microglial processes, resulting in microglia that resemble those seen in awake mice (Fig. 3a). Microglial pseudopodia retracted within the first 30min of imaging (Fig. 3b; two-way ANOVA; $p<0.001$), and new pseudopodia were less likely to be formed (Supplementary Fig.9a). In addition, we also observed a persistent decrease in microglial motility as compared to saline-treated mice (Supplementary Fig.9b; two-way ANOVA; $p<0.01$), despite a return to baseline pseudopodia dynamics in the second half-hour of imaging. To further validate that the effects of β_2-AR agonism were a direct effect on microglia and not due to peripheral activation of β_2-ARs, we directly applied a selective β_2-AR agonist, terbutaline, through an acute craniotomy and replicated our effects from the i.p. clenbuterol administration (Supplementary Fig.10, and Supplementary Video 7).

To further quantify the sustained impact of clenbuterol on microglia in fentanyl-anesthetized mice we traced individual microglia and used Sholl analysis to assay the complexity of the arbor. We found that microglia treated with clenbuterol two hours before imaging had significantly reduced arbor complexity (Fig. 3c–f; AUC one-way ANOVA; $p<0.001$; Maximum # of intersections; one-way ANOVA; $p<0.001$). Three hours post-administration, clenbuterol-treated animals exhibited a significant decrease in microglial process coverage of the parenchyma over one hour of imaging (Fig. 3g,h; one-way ANOVA; $p<0.001$). To assess whether the observed effects of acute clenbuterol administration produced sustained changes in microglial dynamics, we examined microglial motility 3 hours after clenbuterol injection and found it was not significantly reduced (Supplementary Fig. 11, Supplementary Videos 8–10).

To further dissect the effects of β_2-AR signaling on microglial dynamics, we asked whether reducing microglial β_2-AR signaling affected microglial dynamics under fentanyl anesthesia. DSP4 injection 48 hours prior to imaging reduced microglial surveillance (Fig. 3h; two-way ANOVA; $p<0.05$), and decreased microglial motility (Supplementary Fig. 11, Supplementary Videos 11), while administering the β_2-AR antagonist, ICI-118,551 (at the time of imaging) to selectively block β_2-AR signaling had no effect (Fig. 3h,Supplementary Fig. 11, Supplementary Video 12).

β_2-AR antagonism in awake mice increases microglial process ramification

Because β_2-AR agonism decreased microglial ramification and surveillance in anesthetized animals, we wanted to evaluate if similar effects occur without anesthesia. Awake mice imaged through cranial windows were treated with either clenbuterol or ICI-118,551 to selectively stimulate or block β_2-AR signaling respectively (Fig. 4a). Sholl analysis revealed that clenbuterol had no effect on microglial ramification in awake mice (Fig. 4a–c,e; AUC; paired t-test; n.s.; Maximum # of intersections; paired t-test; n.s.) whereas ICI-118,551 increased ramification (Fig. 4a,b,d,f; AUC; paired t-test; $p<0.001$; Max response; paired t-test; $p<0.001$). We found that clenbuterol significantly reduced microglial surveillance of the parenchyma, despite the lack of impact on microglial arborization (Fig. 4g,h; paired t-test; $p<0.01$). We also found that ICI-118,551-treated microglia showed enhanced surveillance of the parenchyma (Fig. 4g,i; paired t-test; $p<0.05$). In addition, we examined motility and found that clenbuterol significantly reduced microglial motility (Supplementary Fig. 12a), while ICI-118,551 significantly increased microglial motility in awake mice (Supplementary Fig. 12b; Supplementary Video 13). Combined with our previous data in awake vs. anesthetized mice, these data suggest that during wakeful conditions, microglial ramification and process motility are inhibited by endogenous NE, and that relieving this inhibition via β_2-AR antagonism induces an increase in process ramification and surveillance recapitulating the effects of anesthesia.

β_2-AR signaling impacts microglial response to focal tissue injury

Previous work has shown that both NE and β-AR stimulation blocks microglial process chemotaxis to ATP *in vitro*[24] suggesting that β-AR signaling may attenuate microglial responses to injury-induced ATP release. To determine whether this is also true *in vivo*, we created a focal laser tissue injury in adolescent fentanyl-anesthetized mice and observed reduced microglial process recruitment to the lesion core in clenbuterol treated mice (Fig. 5a,b; Supplementary Video 14–15). We observed that peak response and overall microglial response to the injury were significantly reduced in clenbuterol-treated mice (Fig. 5c–e; one-way ANOVA; $p<0.0001$). Furthermore, there was a trend towards an increased response in nadolol- or ICI-118,551-treated mice (Fig. 5c–e; one-way ANOVA; $p=0.12$). These data suggest that microglial β_2-AR signaling attenuates not only baseline surveillance, but also the response to changes in CNS homeostasis during acute injury.

Noradrenergic signaling and β_2-AR stimulation impair critical period ocular dominance plasticity.

After observing the robust effects of noradrenergic and β_2-AR signaling on microglia, we asked whether this signaling pathway mediates microglial roles in synaptic plasticity.

Previously published work from our laboratory has shown that microglial processes interact with neural elements *in vivo*[4,7,10] and that these interactions can be modulated by visual experience[4]. We have also shown that during the mouse adolescent visual critical period perturbation of microglial purinergic signaling through P2Y12 impairs ocular dominance plasticity (ODP)[10]. Given the antagonistic effect of β_2-ARs on P2Y12 signaling[24], we hypothesized that microglial β_2-AR signaling might impair ODP during the peak of the mouse visual critical period (~P25-P32[25,26]), when our experiments have demonstrated altered microglial phenotypes (Fig. 1–4). Selectively activating β_2-ARs chronically with clenbuterol effectively blocked ODP, indicated by the lack of ocular dominance shift of neuronal responses after four days of monocular deprivation (Fig. 6a–c; two-way ANOVA; $p<0.001$). As before, nadolol was administered with clenbuterol to block peripheral β_2-AR stimulation. Both saline-treated and nadolol-only treated animals showed normal ocular dominance shifts indicating intact ODP (Fig. 6b,c). In addition, cortical NE depletion with DSP4 treatment impaired ODP confirming previous work demonstrating that NE has important roles in ODP (Fig. 6c)[27]. However, this effect appeared to be independent of β_2-AR signaling as chronic blockade of β_2-ARs with ICI-118,551 did not impact ODP (Supplementary Fig.13). Thus, sustained stimulation of β_2-AR signaling interferes with the plastic processes that mediate ODP, but NE signaling through other signaling pathways are necessary for ODP[28]. β_2-AR stimulation may impair ODP by modulating microglial surveillance and limiting microglial interactions with synapses. To examine this possibility, we utilized CX3CR1^{GFP}/THY1^{YFP} mice to simultaneously image microglia and dendrites in visual critical period mice. We found that β_2-AR stimulation, but not depletion of NE, significantly reduced microglial contacts with dendritic spines (Fig. 6d, e). This suggests that the effects of β_2-AR stimulation on ODP may arise, in part, from abnormal microglial dendritic spine interactions while depleting NE likely affects plasticity through other cell-types.

Microglial β_2-AR activation impairs ocular dominance plasticity

Despite the known roles of microglia in ODP and high microglial β_2-AR expression, it is possible that pharmacological β_2-AR stimulation impairs ODP through non-microglial pathways. To determine whether the observed results were specifically mediated through β_2-AR signaling in microglia, we crossed the CX3CR1Cre-ERT[9] mouse line to β_2-AR floxed mice[29] to selectively ablate β_2-ARs in microglia (Fig. 7a). Mice were dosed with tamoxifen from ~p2–4[9] to ensure that β_2-ARs were selectively ablated from microglia in adolescent mice. Microglia were isolated from tamoxifen-treated animals and successful gene excision of β_2-ARs confirmed by PCR (Supplementary Fig.14). To test whether the effects of β_2-AR stimulation on microglial dynamics were dependent on microglial β_2-AR expression, we labeled microglia by crossing these mice with the tdTomato Ai9 reporter line. Clenbuterol no longer induced a retraction of the microglial arbor in tamoxifen-treated Cx3cr1Cre-ERT-Het/β_2-ARflx/Ai9 mice, while the response was intact in control, tamoxifen-treated Cx3cr1Cre-ERT-Het/Ai9 mice (Fig. 7b,c; two-way ANOVA; $p<.0001$), further confirming loss of these receptors from microglia. Importantly, we also found that the effects of DEX on microglial arborization were also lost in the Cx3cr1Cre-ERT-Het/β_2-ARflx/Ai9 mice, further indicating that microglial β_2-ARs are essential regulators of microglial responses to NE (Fig. 7d–f & h–j). We then repeated ODP experiments with tamoxifen-treated Cx3cr1Cre-ERT-

Het controls and Cx3cr1Cre-ERT-Het/β_2-ARflx (Cx3cr1Cre/β_2-ARflx) mice (Fig. 7g,k). Control mice showed the same effects of pharmacological manipulation as C57BL/6J mice (Fig. 7g; two-way ANOVA; $p<0.05$). Cx3cr1Cre/β_2-ARflx mice lacking microglial β_2-ARs exhibited normal ODP, suggesting that microglial β_2-ARs are not necessary for ODP. We found that ablating β_2-ARs in microglia, however, rescued ODP during chronic clenbuterol administration (Fig. 7k; two-way ANOVA; n.s. interaction), suggesting that aberrant activity of microglial β_2-ARs interferes with normal plasticity. DSP4 treatment still blocked ODP in the Cx3cr1Cre/β_2-ARflx mice (Fig. 7k; two-way ANOVA; Bonferroni post-hoc; $p<0.05$), suggesting that the effects of depleting NE are mediated by other cell types. Thus, we confirmed that chronic stimulation of microglial-specific β_2-ARs is capable of blocking ODP while cortical NE depletion likely blocks ODP through non-microglial mechanisms.

Discussion

We report that the microglial β_2-AR is a key receptor in regulating basal microglial surveillance and injury response in the visual cortex of awake mice, and that chronic pharmacological stimulation of this receptor during the mouse adolescent visual critical period impairs cortical experience-dependent plasticity. In wakeful conditions, microglial process arbors are small and highly motile, dominated mostly by filopodial protrusions. Anesthesia rapidly increases microglial arborization and pseudopodia extension allowing microglial processes to survey a larger area of cortex and respond more rapidly to a focal injury. Administration of the β_2-AR agonist clenbuterol in anesthetized mice results in microglial characteristics that resemble the awake state, while the β_2-AR antagonist ICI-118,551 generates microglial phenotypes that resemble anesthetized conditions in awake mice. Furthermore, ablation of β_2-ARs in microglia eliminates morphological changes between awake and anesthetized states suggesting that signaling through this microglial receptor regulates microglia function during wakefulness. Our findings indicate that there are robust differences in microglial basal dynamics between awake and anesthetic states and that these changes are driven by noradrenergic β_2-AR signaling in microglia (Supplementary Fig. 15).

Endogenous NE is a potent modulator of microglial function

NE is a potent neuromodulator that regulates brain function and elicits transitions between internal states such as wakefulness, arousal, and stress. NE has many targets throughout the nervous system and can coordinate synchronized changes in multiple cell types through tonic signaling and phasic firing to salient or noxious stimuli.[19] Astrocytic function, for instance, is highly dependent on brain state with different roles during sleep, when NE is low, and wakefulness or stress, when NE is high[23]. Here we provide evidence that microglia, like astrocytes, may differ robustly between the awake and anesthetized state. While we could not quantify microglial dynamics in sleeping animals, due to the fact that mice have very short sleep cycles[23,30], our experiments with DEX suggest that microglia may also show enhanced surveillance and injury responses during sleep. DEX is thought to hyperpolarize LC neurons and inhibit NE release throughout the brain[21], leading to brain activity that resembles more prolonged slow-wave sleep in humans[30]. The idea that microglia behave differently in the awake vs. sleeping brain merits further investigation, as

many diseases are linked to changes in sleep patterns, and the quality of sleep can in turn greatly impact disease progression[31].

Noradrenergic inhibition of microglial dynamics impairs synaptic plasticity, suggesting that brain state, through noradrenergic signaling, modulates microglia-synapse interactions[4]. Simulating a chronic awake state through pharmacological targeting of microglial β_2-ARs prevents ODP, further suggesting that microglia require decreased noradrenergic signaling in order to fulfill essential roles in neural plasticity. This implies that in physiological conditions NE may be exerting an important inhibitory function on microglia, perhaps preventing inappropriate or excessive microglia-neuron interactions. Our findings also suggest that increased noradrenergic signaling due to sleep deprivation or genetic conditions altering β_2-AR signaling may result in aberrant microglial participation in plasticity processes. In the awake state, tonic NE release decreases neural variability in firing rates and is thought to enhance the signal-to-noise ratio in the visual cortex[32]. NE bulk release from varicosities could enhance neural tuning while simultaneously inhibiting microglial-neuron interactions through selective activation of β_2-ARs. Previous work has demonstrated that sleep is necessary for plasticity, as well as specifically for ODP[33], and while a multitude of signals are regulated by sleep, microglial β_2-AR signaling may be an additional target. It is also important to note that microglial P2Y12 is necessary for ODP and both genetic and pharmacological inhibition results in the loss of plasticity[10]. Thus, it is likely that interactions between β_2-AR and P2Y12 signaling in microglia regulate microglial roles at synapses. Effects of NE on microglia and plasticity may also be mediated by NE signaling in other cell types. In our study, depletion of NE with the neurotoxin DSP4 blocked ODP and affected microglial motility, however ablation of microglial β_2-ARs failed to rescue plasticity in DSP4 treated mice. This suggests that loss of NE in this model signals through a different receptor or cell-type to alter microglial dynamics and plasticity. Interestingly, astrocytes have robust expression levels of α_1, α_2, and β_1, ARs which contribute to astrocytic metabolic coupling and K+ clearing during neural activity[19]. The diverse effects of NE on astrocytic function could make astrocytes an intermediary by which depletion of NE may be altering both microglial function and neural plasticity. It is also important to note that other signaling pathways affected by NE may also affect microglia. The regulation of glymphatic flow by wakefulness, for instance, may be an additional mechanism by which NE signaling in other cell types may influence microglial dynamics, in this case by altering extracellular space[16], though the extent to which extracellular space increases during wakefulness remains unclear[34].

Intracellular signaling effectors of β_2-AR in microglia

β_2-AR and P2Y12 signaling have opposite effects on microglial morphology, chemotaxis[35] and ODP. Both receptors are G-protein coupled. While P2Y12 is coupled to the G_i subunit, the β_2 AR is coupled to G_s, suggesting that these may act in a push-pull system[24] (Supplementary Fig. 15). The intracellular pathways that mediate G protein signaling in microglia have recently garnered interest. E*x vivo*, β_2-AR stimulation by NE and β_2-AR agonists blocks P2Y12 process chemotaxis toward ATP by downstream protein kinase A (PKA) dependent phosphorylation of phosphoinositide 3-kinase gamma (PI3Kγ)[24,36], suggesting this pathway may be important. Interestingly, downstream cAMP has been

elucidated as a key regulator of the dynamic shifts in microglial processes between filopodial and pseudopodial protrusions[22]. Microglial G_s coupled receptors including β_2-ARs promote cAMP accumulation thereby driving a filopodial rich phenotype which alters microglial dynamics and surveillance[22]. Recent studies in the acute brain slice have shown that baseline microglial motility relies on the maintenance of the microglial resting membrane potential by the two-pore domain channel THIK-1[37,38]. Genetic or pharmacological perturbations of THIK-1 function reduce microglial ramification and surveillance, similarly to β_2-AR stimulation, making it another likely target. While P2Y12 signaling does not alter basal surveillance in microglia, it does gate THIK-1 function causing hyperpolarization in response to ATP. β_2-ARs could similarly interface with THIK-1 or Kir K^+ channels to alter the microglial resting membrane potential thereby inhibiting surveillance. This is the case in neurons of the medial prefrontal cortex, where clenbuterol hyperpolarizes fast-spiking GABAergic interneurons[39] due to β_2-AR driven $G_\alpha s$ inhibition of inward Kir K^+ rectifying channels. β_2-ARs could also regulate microglial motility through recruitment and signaling by β-arrestin1 and 2 which are both expressed in mouse microglia[40] and can have diverse downstream targets including cytoskeletal proteins[41]. Recent work in zebrafish showed a critical role of β-arrestin1 in maintaining normal microglial morphology, surveillance, and phagocytosis[42]. Long-term activation of β_2-ARs can lead to heterologous desensitization and possible endocytosis of other GPCRs such as P2Y12[41] through β-arrestins. Activation of β-arrestin2 in microglia initiates longer term anti-inflammatory signaling through blockade of Mitogen-activated protein kinases (MAPKs) rescuing neuronal death in a Parkinson's disease model[43]. P2Y12 signaling can also drive IL-1β and inflammasome recruitment in response to LPS triggered inflammation[37], suggesting that cytokine effectors may critically alter microglial and inflammatory milieu after activation of GPCRs. It is important to note that many forms of plasticity[44], including ODP[45], are thought to be mediated by cytokines, such as IL-1 β and TNFα, which are also known to promote sleep[46]. If microglial β_2-AR signaling is also regulated by sleep-wake cycles, then microglial β_2-ARs may in turn also alter sleep through regulation of cytokine production driven by downstream nuclear factor ϰβ signaling[47]. It is important to note that the majority of our experiments are carried out in mice haploinsufficient for CX3CR1. While CX3CR1 loss does not affect microglial morphology, motility, contact with synapses or ODP[48], interactions between NE and fractalkine signaling have been reported[49], making it possible that effects of NE may be more or less pronounced in WT mice. Additionally, while the pharmacological agents used highly specific, off target effects are always possible. However, previous work and our findings, paint an emerging picture of a delicate interplay between P2Y12 and β_2-AR signaling which mediate the responsivity of microglia to acute perturbations in the CNS milieu.

While our work has explored the effects of β_2-AR signaling on microglial physiology, the diversity of intracellular signaling pathways down-stream of microglial β_2-ARs make this receptor a fascinating target for the gating of microglial physiology and responses in the context of disease. Sleep disturbances are a hallmark of neurodegenerative diseases[50]. Interestingly, prolonged wakefulness and increased noradrenergic signaling prevent adequate astrocyte-driven glymphatic clearance of Aβ[16]. While we found that acute noradrenergic signaling inhibits microglial recruitment to acute tissue damage, NE may be helpful in

mediating microglial responses to chronic degenerative disease states. While more work is needed to understand NE's role in mediating microglial function in health and disease, altogether, our data show that microglial β_2-ARs are potent regulators of microglial dynamics and visual system experience-dependent plasticity. Our study provides promising evidence that microglia have critically different roles in the anesthetized and awake brain.

Methods:

Animals.

Experimental protocols were carried out with the approval of the Institutional Animal Care and Use Committees of both the University of Rochester and Massachusetts Institute of Technology and conformed to the National Institute of Health guidelines. Experiments were conducted on male and female mice with a C57/Bl6 background between P21-P120. CX3CR1-GFP[51](JAX: 005582) heterozygous mice were used to visualize microglia for *in vivo* two-photon imaging. CX3CR1-GFP mice were also crossed to THY1-YFP[52] (JAX: 003782) mice to visualize both microglia and dendritic spines for spine contact imaging. CX3CR1-Cre^{ERT} [9] (JAX: 021160) mice were bred to Adrbeta2-flox[29](Karsenty Laboratory courtesy of the Rosen Laboratory) mice to generate mice which had β_2ARs selectively knocked out of microglia. CX3CR1-Cre^{ERT} mice were also bred to Ai9[53] (tdTomato JAX: 007909) mice for visualization of microglia in 2-photon experiments. Mice were housed with a standard 12:12 light/dark cycle and fed standard chow *ad libitum*. For experiments regarding ocular dominance plasticity, mice were used in the visual critical period (P25–35). Sex distribution is provided in Supplementary Table 1, exact n's for all experiments can be found in the legends to all figures. More information can be found in the Life Sciences Reporting Summary.

Stress Exposure.

For stress exposure experiments, male and female mice were randomly assigned to control or stressed cohorts. Stressed mice were briefly anesthetized using 3% isoflurane and restrained in 50ml conical tubes drilled with air holes in a brightly lit fume hood for 2 hours. This stress period was repeated for three consecutive days at approximately the same time each day. Following the third day, mice were either imaged immediately following or 4 hours after the final stressor. Control mice were handled on each day but returned to their home cages.

Circadian Rhythm Measurements.

For circadian rhythm experiments, mice were kept at the standard 12:12 light/dark cycle with lights on at 6:00 and lights off at 18:00. For fixed-tissue analysis, brains were collected at 6:00, 12:00, 18:00, and 24:00. For *in vivo* experiments, animals were imaged at 12:00 and 24:00. For collection times during the dark cycle, cages were covered with a black sheet to minimize light exposure before experiments.

Flow isolation of microglia and confirmation of β_2AR excision.

We utilized our previously published experimental design[54] with a small modification to accommodate for the YFP expression in the CX3CR1-Cre^{ERT} line. CX3CR1-Cre^{ERT}/

Adrbeta2-flox mice were either dosed with 50μg tamoxifen from P2–4 or undosed. At ~P28 mice were euthanized by an i.p. sodium pentobarbital overdose (Euthasol, Virbac) and transcardially perfused with ice cold 0.15 M PBS. Each brain was removed and the whole cortex was dissected from the rest of the brain in ice cold, degassed FACS buffer (0.5% BSA, Sigma A2153 in 1× PBS Invitrogen 20012–027 pH 7.2). The tissue was kept on ice throughout all the procedures. Cortices were homogenized with a Dounce homogenizer and then passed through a 70μm filter and centrifuged (210xg, 7min, 4 °C). The supernatant was aspirated from the pellets and then the pellets resuspended and prepared for magnetic sorting with Myelin Removal Beads II (Miltenyi 130–0960733). The resuspended labelled tissue was passed through a 70μm filter and then the FACS buffer primed Magnetic columns (Miltenyi 130-096-733). After passage through the magnetic columns the samples were centrifuged, the supernatant removed, and resuspended in FACS buffer with Fc block (Biolegend 101320) for 15min at 4 °C.

Samples were incubated with CD11b-AlexaFluor BV786 (1:200, BD Biosciences 740861, clone: M1/70) and CD45-APC (1:400, BD Biosciences 561018, clone: 30-F11) for 30 min in the dark at 4°C. Each sort included the following compensation controls: BV720 bead control, APC bead control (eBiosciences 01-111-42), unstained live cells, and propidium iodide (PI) labelled Triton X-100 killed cells. An additional fully-labelled sample was prepared with spare tissue to check the voltage settings prior to running experimental samples. All samples were run on an 18-color FACS Aria II flow cytometer. For the sort, all samples and controls were resuspended in 300μl FACS buffer. PI was added to the samples just prior to sorting. An example of a microglial sort can be found in Supplementary figure 8. More information can be found in the Life Sciences Reporting Summary.

Cells were collected in PBS for DNA isolation with a Qiagen DNAeasy DNA isolation kit. A total of 3 tamoxifen-treated and 3 tamoxifen-untreated animals were included in our confirmation experiments. Isolated DNA was run through 2 PCR protocols, 1st the PCR for confirmation of floxed allele presence (550BP product: Fw: ccaaagttgttgcacgtcac, Rv: gcacacgccaaggagattat), and 2nd excision confirmation (~800BP: Fw: ccaaagttgttgcacgtcac, Rv: aagaaagaggaggggctgag)[29]. We confirmed that in tamoxifen-treated mice the 550BP floxed allele PCR product was no longer present (Supplementary figure 8), and the excision product ~800BP was present. In our untreated mice we still had the 550BP floxed allele, however we did also see the ~800BP excision product in the second PCR. This suggests that there is a certain degree of leakiness in our Cre expression. However, this leakiness did not affect our experimental outcomes as our controls for all CX3CR1-Cre^{ERT}/Adrbeta2-flox experiments were CX3CR1-Cre^{ERT}-HET mice dosed with tamoxifen.

Pharmacological Agents—Fentanyl cocktail[4,7,10,48]: fentanyl (0.05mg kg^{-1}, i.p.), midazolam (5.0 mgkg^{-1}, i.p.), and dexmedetomidine (0.5 mgkg^{-1}) Pre-mixed and given i.p. Used for anesthetized 2-photon imaging sessions and for thin-skull and cranial window procedures. Dexmedetomidine[21]: 0.4 mg kg^{-1}, i.p. for 2-photon imaging. Atipamizole: 0.2mg kg^{-1}, i.p. was used to reverse dexmedetomidine anesthesia.

Clenbuterol[55] (Sigma, 21898-19-1): 1–5 mg kg^{-1}, i.p. for 2-photon imaging and 5 mg kg^{-1}, i.p. once every 12hrs for 4 days for iOS. Nadolol[56](Sigma, 42200-33-9): 10 mg kg^{-1}, i.p. for

2-photon imaging and once every 12hrs for 4 days for iOS. ICI 118,551[57] (Sigma, 72795-01-8): 10 mg kg^{-1}, i.p. for 2-photon imaging and 8 mg kg^{-1} day^{-1} by mini-osmotic pump for 4 days (Alzet, 1007D) for iOS. N--N-ethyl-2-bromobenzylamine (DSP4)[58] (Sigma, 40616-75-9) : 50 mg kg^{-1}, i.p. twice at 48hr intervals a minimum of 48 hours prior to either 2-photon imaging or to the deprivation period of iOS. Tamoxifen (Sigma, 10540-29-1): 50μg by intragastric gavage once daily from ~post-natal day 2–4 in experiments utilizing CX3CR1-Cre^{ERT} mice[9].

Monocular deprivation.

Animals were randomly assigned to ND or 4MD cohorts starting from P27±2. MD animals were anesthetized (isoflurane, 5% induction, 3% maintenance). The right eyelids were trimmed and antibiotic eye ointment was applied to the eye and trimmed margins. The eye was then sutured closed. Mice were monitored and given carprofen (5 mg kg^{-1}) every 24 hours for analgesia as needed. The eye was not reopened until the day of imaging and any animals with a compromised eye or sutures were excluded from the rest of the experiment.

iOS Imaging.

These experiments utilized C57/Bl6, CX3CR1-Cre^{ERT}-HET, and CX3CR1-Cre^{ERT}-HET/Adrbeta2-flox mice. Following 4 days of ND or MD, animals were re-anaesthetized with isoflurane and chloroproxithene (2 mg kg^{-1}), and sutured eyes reopened. The skull over contralateral visual cortex was exposed, cleared, covered with agarose (0.25%) and sealed with a coverslip. Animal anesthesia was maintained with isoflurane (0.75%) throughout imaging. A custom-made iOS imaging set-up was used to record activity in the visual cortex during presentation of a visual stimulus (DALSA 2M30 CCD). The cortex was illuminated with 550-nm light to identify vasculature and 700-nm light for iOS collection. Images of the left visual cortex were collected continuously, while either the ipsilateral or contralateral eye was stimulated by white horizontal square-wave bar gratings on a black background moving upwards (90°) or downwards (270°) at a frequency of 8°/s for 6min (30 cm from eyes). Visually evoked responses were collected for each eye individually. The normalized amplitude of the fast Fourier transform component of the intrinsic signal was averaged for each eye from responses to both stimulus directions and compared between eyes offline using MATLAB to determine ocular dominance. An ODI was computed using the following equation: ODI=(average contralateral response-average ipsilateral response)/(average contralateral response/average ipsilateral response).

Acute cortical slice preparation—Cx3cr1-GFP heterozygous mice were decapitated and the brain was rapidly removed and placed into ice-cold artificial cerebrospinal fluid (ACSF) containing (in mM): 126 NaCl, 2.5 KCl, 1.25 KH2PO4, 10 glucose, 1.3 MgSO4, 26 NaHCO3, 2.5 CaCl2, and constantly oxygenated (95% O2, 5% CO2). Coronal sections 400 um thick were prepared using a vibratome (Vibratome 1000) with the brain submerged in ice-cold oxygenated ACSF. Sections containing visual cortex were transferred to oxygenated ACSF at ambient temperature until imaging (between 30 minutes and 2 hours). Slices were placed in a perfusion chamber (Warner) and perfused with 1–2 mL per minute oxygenated ACSF heated to 37C using an inline heater (Warner), and cortical GFP-expressing microglia were imaged at a depth of 50–100 um below the surface using a two-photon microscope. An

initial time series of Z stacks was taken every 5 mins for 30 mins in slices perfused with ACSF. The perfusion solution was then switched to ACSF containing 100 nM dexmedetomidine (Tocris) or normal ACSF, allowed to incubate for 20 minutes, and then Z-stacks of the same area were taken every 5 mins for 30 minutes. Motility was analyzed as described below.

Cranial Window Surgery.

Animals were anesthetized using the fentanyl cocktail during the cranial window implantation surgical procedure. Lubricant ointment was used to keep the eyes moist and protected. Body temperature was maintained at 37°C during the surgery. Aseptic technique was adhered to during all surgical procedures: all tools were autoclaved for steam sterilization, and tools were sterilized in a bead sterilizer between surgeries (up to 3 uses). Mice were mounted in a stereotaxic frame and head-fixed for surgical procedures. The skull was exposed through a scalp incision and all connective tissues were cleared off the skull. A 3mm biopsy punch (Integra) was then used to create a circular score on the skull over V1. A 0.5 mm drill bit (FST) was used to then drill through the skull for the craniotomy, tracing the 3mm score. A 5mm coverslip attached to a 3mm coverslip (Warner Instruments) by UV glue (Norland Optical Adhesive, Norland Inc) was then slowly lowered down into the craniotomy (3mm side down). The coverslip was carefully secured with Loctite 404 glue (Henkel Corp). A custom headplate produced by emachine shop (www.emachineshop.com) (designs courtesy of the Mriganka Sur Lab, MIT) was then secured onto the skull utilizing C&B Metabond dental cement (Parkell Inc). The cement was then used to cover the rest of skull and seal the incision site. Animals were administered slow-release buprenex by URMC veterinary staff (s.q. 5 mg kg^{-1} every 72 hours) and monitored for 72 hours post-op.

Two-Photon Microscopy—A custom two-photon laser-scanning microscope was used for *in vivo* imaging (Ti:Sapphire, Mai-Tai, Spectra Physics; modified Fluoview confocal scan head, 20× lens, 0.95 numerical aperture, Olympus). Excitation for fluorescent imaging was achieved with 100-fs laser pulses (80MHz) at 920nm for GFP and 1020nm for tdTomato with a power of ~40mW measured at the sample. For motility experiments in CX3CR1-GFP mice a 580/180 (GFP) filter was used. For experiments in CX3CR1-Cre+/Ai9 mice a 565 a 578/105 filter was used. During anesthetized cranial window imaging sessions mice were anesthetized with our fentanyl cocktail. Prior to awake imaging sessions mice were trained for three consecutive days in head-restraint on a running wheel progressing from 30 minutes to 1 hour of head-restraint over the three days. During awake imaging sessions mice were head-restrained and kept on a foam running wheel for the duration of the session, the restraint apparatus and wheel were the same as were used in the initial training sessions. During thin-skull[4,10,48] imaging sessions mice were anesthetized with the fentanyl cocktail prior to the skull-thinning surgery and for the duration of the imaging session. During imaging sessions and during post imaging recovery mice were kept at 37°C until they were alert. Imaging was conducted at 3–5 digital zoom and 1um z-step, with time-lapse imaging at 5-minute intervals over 1 hour with the exception of spine contact imaging which was conducted at 8 digital zoom. Image analysis was done offline using ImageJ and MATLAB with custom algorithms as described in Sipe et al. 2016 and available on the Majewska Laboratory website through GitHub.

Microglial Morphology: For *in vivo* morphological analysis 3–5 microglia were selected per animal from a single time-point in the imaging session. For paired time-course experiments utilizing dexmedetomidine and atipamezole the same microglia was selected from the beginning of the first treatment condition, and then 15 minutes into the second session. For all other experiments microglia were selected from the same time point of the imaging sessions for consistency. For each microglia selected an individual z-projection was created in ImageJ, which encompassed the entire microglial arbor. All the microglial processes were manually traced and then the tracing of the processes was subjected to sholl analysis. Because of the limits of manual tracing small filopodia may have been missed. For each animal an average of the 3–5 microglia selected was found and that average represented the value for that animal. The area under the curve of the Sholl profile and then maximum intersection number were found and analyzed as indices of microglial arbor complexity.

Microglial motility and surveillance: Microglial motility analysis was performed in ImageJ and MATLAB as previously described[7,10]. Z-stacks were collected in V1 every 5 minutes for 1 hour, producing 12 time points. The dexmedetomidine time course experiments were collected as a first portion either awake or under dexmedetomidine for 20minutes and then 1 hour immediately post-dexmedetomidine or atipamezole. All z-stacks were between 60–120μm and for analysis average intensity z-projections were made (30–40μm thick). Lateral motion artifact and photobleaching was corrected prior to analysis (Stackreg plugin, ImageJ). A custom MATLAB algorithm[7,10] was used to compare pixels across individual time points and across consecutive time points to generate a motility index (defined as the sum of all changed pixels by the unchanged pixels). Our motility script in MATLAB compares consecutive time-points across the 5 minute imaging intervals and calculates differences in pixels: pixels present in the first time point and absent in the second are defined as retractions and pixels absent in the first time point and appearing in the second are defined as extensions. The retractions and extensions are summed and divided by the stable pixels for each of these consecutive time point pairs to generate motility indices for each of the pairs. The final motility index that we show for our conditions represents the average of the motility indices calculated for each of the pairs. For the motility index, all microglia in the Z-projection of the imaging session were analyzed to generate the value per animal for the 1-hour session. The thresholded time points were also used to calculate the area monitored (surveillance measurement) by microglia during the 1-hour imaging session. This was done by collapsing the 12 time points through the maximum intensity z-projection function in ImageJ and calculating the total number of pixels representing microglia out of the total pixels in the field of view. The surveillance ratio was defined as the ratio of microglia occupied pixels out of the total pixels in the image.

Microglial pseudopodia measurements: For pseudopodia analysis t=0, t=30, and t=60 minutes from the motility imaging sessions were used to create 0–30- and 30–60-minute overlays. The number of pseudopodia were then counted using the multipoint tool in imageJ to track marked pseudopodia. Pseudopodia were identified as round, bulbous projections with width greater than the parent processes from which it protruded (typically ~2–3 μm in diameter). Conversely, filopodia were identified as thin, acute processes tapered at the tip with width lesser than the parent process (typically <1 μm in width). Pseudopodia were

identified for counting based on their round morphology and their presence at the end-tips of the processes. Retraction (retracted pseudopodia/total pseudopodia) and extension ratios (extended pseudopodia/total pseudopodia) were calculated based on the number of retracted or extended pseudopodia divided by the total pseudopodia counted. Because comparisons were made over 30 minutes (overlays of 0–30 and 30–60 minutes), and pseudopodia are transient, all pseudopodia fell into the category of either retracted (purple in Fig. 3a) or extended (green in Fig. 3a), providing a clear measurement of the tendency of processes to either extend or retract after treatment. For imaging of Ai9 animals, only 0 and 30 minute timepoints were taken as the tdTomato fluorophore suffered from pronounced photobleaching with repeated imaging. This precluded the use of Ai9 for motility measurements.

Terbutaline Motility: For direct application of terbutaline to the brain parenchyma, small craniotomies were performed on anesthetized animals and imaged directly without a coverslip. Baseline imaging was collected every 2 minutes for 30 minutes in a sterile saline objective immersion. Following baseline, immersion media was either replaced by additional sterile saline, or terbutaline in sterile saline (1mM) to allow for pharmacological diffusion into the brain parenchyma and imaged for an additional 60 minutes. Baseline periods and saline treated animals controlled for microglial activation due to craniotomies and animals that had significant motility or morphological changes during the baseline were removed from the study.

Laser Ablation: Laser ablation injuries were created by running a point scan for 8s at 780nm using ~75mW at the sample. The microglial injury response was imaged by collecting Z-stacks of 50–90μm every 5 minutes. For analysis, z-projections were all comprised of 10μm of the stack, encompassing the approximate center ablation core. The file was converted to an avi and subjected to analysis by a custom MATLAB script designed to calculate the movement of microglial processes towards the ablation core. Briefly, for each pixel at each time point the script generates a vector which estimates the magnitude and direction of motion of the pixel utilizing the Farneback method for estimating optic flow[59]. To ensure that our analysis concentrated on the number and magnitude of responding processes, we excluded vectors not directed towards the core as well as vector magnitudes below 5 pixels of motion. This was necessary to filter out noise pixels which represent artefacts such as motion and tissue distortion upon initial ablation. To quantify the generated vectors we summed the magnitudes of all the vectors at each time point and normalized this value to the total number of pixels in the image. The first time-point was excluded from all analysis as the script estimates the first time point's movement by assuming a blank frame preceding the first time point. We then found the area under the curve for our injury response normalized magnitude as well as the maximum value of our normalized magnitude over the 1hr session.

Microglial dendritic spine contact analysis.

In order to visualize microglial contacts with dendritic spines the GFP channel was assigned the color green and the YFP channel was assigned the color red. Microglial contacts with dendritic spines were identified by manually stepping through the Z-stack of the merged

channels. Contact was identified as the colocalization of the fluorescence of microglial and dendritic elements. For each animal 40–60 spines were evaluated for microglial contact (this represents the range of total spines typically visible for the duration of an entire imaging session). The proportion contacted in the analysis was quantified as the number of contacted spines out of the total spines counted.

Resonance Imaging.

Animals were head-fixed and imaged with a 16× objective with an 8× digital zoom at 38 fps with 8-raster averages resulting in effectively 4 fps. A z-piezo was used with a commercial two-photon microscope using proprietary software (Prairie View, Prairie Technologies Inc., Bruker Corporation) to capture 5 planes, 5um apart. Each stack was therefore captured at approximately 1.2s at a resolution of 800×400 and using a Ti:Sapphire (Mai Tai) laser tuned to 910nm. Baseline dynamics were captured for 15 minutes, followed by injection of dexmedetomidine (300ug/kg, s.c.) and immediate imaging for another 30 minutes. For analysis, 5 minute averages were collected and overlaid as magenta and green for each timepoint pairs. Pseudopodia and filopodia were counted in each frame and binned as either extension or retraction of each time. Process velocity and net distance were also computed using the manual tracking plugin (ImageJ).

Optogenetic Stimulation of NE Axons.

CX3CR1-GFP/TH-Cre mice were generated and injected with 400nl AAV1-EF1a-double-flox-hChR2(H134R)-mCherry bilaterally in the locus coeruleus. A cranial window was then created over V1. Viral expression was allowed to reach the cortex over 5 weeks prior to imaging. Animals were then injected with dexmedetomidine (300ug/kg) and allowed to sit in their home cage for 15 minutes before being head-restrained and imaged. Frames were collected using a 16× objective at 800×400 resolution with 2 frames averaged per z-stack resulting in 2.05 fps at 4× digital zoom. 40–60 z-stacks were collected 5um apart at 910nm. Baseline imaging was performed for 30 minutes without interlaced laser stimulation at 10×3 minute intervals followed by 30 minutes of alternating laser stimulation (MBL-7-473-300mW, Opto Engine LLC, 473nm, 6×2s pulses @ 5mW) over 60s followed by 90s of imaging and 30s of buffer time through the objective. CX3CR1-GFP mice without TH-Cre were subjected to the same imaging and light exposure paradigm and served as a light control for the optogenetic experiments.

Code Availability.

MATLAB code for motility and laser ablation analysis is freely available at https://github.com/majewska-lab. More information can be found in the Life Sciences Reporting Summary.

Histology.

Whole brains were collected following transcardial perfusion and overnight post-fixation with paraformaldehyde (4%). Tissue was cryoprotected and coronal sections were cut on a freezing microtome (Microm; Global Medical Instrumentation, Ramsey, MN) at 50-μm thickness. Sections were processed free-floating at room temperature (RT). Briefly, sections

were rinsed, and endogenous peroxidase activity and nonspecific binding blocked with a 10% BSA solution. Sections were then incubated in a primary antibody solution for microglial morphology in circadian experiments (24 h, 4°C, anti-Iba-1, 1:1,000, Wako #019–19741) followed by secondary antibody solution (4 h, RT, Alexa-Fluor 488, 1:500, Invitrogen), mounted and coverslipped. For examination of microglial ramification in circadian rhythm experiments, sections containing primary visual cortex were identified and imaged on a Zeiss LSM 510 confocal microscope (Carl Zeiss, Thornwood, NY). For each section, a 10um z-stack in the center of the tissue was collected with a z-step of 1 um at 40× magnifications. Analysis was performed offline in ImageJ. Z-stacks were smoothed and compressed into a single z-projection. For analysis of ramification, microglia whose entire process arbor was contained within the image were individually selected and cropped into a new image. In the circadian rhythm morphology study 5 microglia from 3 fields of view, for a total of 15 microglia were analyzed per animal. Each image was thresholded to generate a binarized outline of the process arbor, filtered to remove artifacts and analyzed with an automated Sholl analysis plugin (kindly provided by the Anirvan Ghosh laboratory, UCSD).

For analysis of noradrenergic fiber depletion after DSP4 administration whole brains were collected from animals 48 hours and 6 days after the second dose of DSP4. Tissue was processed for histology as described above. Sections were incubated in a primary antibody solution to label noradrenergic fibers[60] (overnight, 4°C, anti-tyrosine hydroxylase, 1:400, Millipore #3122928, clone: LNC1), followed by a secondary antibody solution (2h, RT, Alexa-Fluor 594), mounted and coverslipped. Epifluorescent images of visual cortex containing noradrenergic fibers were then collected utilizing an Olympus Bx51 (Olympus, 40×/0.75) with Spot Pursuit digital camera and Spot Advanced software. Images were binarized in ImageJ to outline the fibers, using the average pixel intensity multiplied by 1.6 as a threshold value for binarization. Total number of white pixels was then measured. Results from 4–5 sections per animal were averaged.

For quantification of microglial labeling in CX3CR1-Cre^{ERT}/Ai9 mice, tissue was processed as above. Epifluorescent images of visual cortex with microglia in red were then collected utilizing an Olympus Bx51 (Olympus, 10×/0.30) with Spot Pursuit digital camera and Spot Advanced software. Any white matter was cropped out of the image. Microglial cell bodies were marked in ImageJ using the paintbrush tool. Results from 4–5 sections per animal were averaged, with a correction for cropped area. Density calculated at number of microglia/area in visual cortex for tamoxifen treated and control groups.

Corticosterone ELISA—Whole-trunk blood was collected in EDTA-lined tubes, centrifuged 10 minutes, 3000 rpm @4°C. Plasma was aspirated from the pellet and stored at −20°C until analyzed. Circulating plasma corticosterone was quantified using a competitive enzyme-linked immunosorbent assay (ELISA) kit (EIACORT, ThermoFisher). Samples were run in duplicate and compared to a standard curve according to kit instructions. Final concentrations for each animal were the average of duplicate reads on a standard plate reader (iMark, Bio-Rad Laboratories Inc.).

Statistics.

Statistical comparisons were made between animal cohorts using Prism VI statistical analysis software. (GraphPad, La Jolla, CA). No statistical methods were used to pre-determine sample sizes, but our sample sizes are similar to those reported in previous publications from our lab[4,10,48] and other publications in the field. N's were also chosen such that we could determine if sex impacted our experimental results, thus sufficient males and females were included to meet this need. All n-values represent individual animals. For analyses where multiple microglia were assayed per animal, all microglia analyzed for an individual animal were averaged to generate a single value per animal. Animals were randomly assigned to conditions with the caveat of an effort being made to evenly distribute males and females amongst the various groups. Where possible in repeated imaging experiments conditions were randomized to account for potential ordering effects. All analyses were conducted blind to the experimental condition. Animals were only excluded from analysis if an imaging session could not be completed in full, otherwise all completed imaging sessions collected were utilized. All values reported are the mean± s.e.m. For all analyses, α=0.05. Two-tailed unpaired, or paired t-tests and one-way or two-way ANOVAs with or without repeated measures (ANOVA, RM-ANOVA, respectively) with Holm-Sidak multiplicity corrected post hoc comparisons were used to compare cohorts where appropriate. The data met the assumptions of normality and equal variances as tested by Prism VI as part of the statistical analyses. More information can be found in the Life Sciences Reporting Summary.

Data Availability.

The data that support the findings of this study are available from the corresponding author upon request.

Supplementary Material

Refer to Web version on PubMed Central for supplementary material.

Acknowledegements

We thank the University of Rochester Medical Center Flow Core for their expert training and services. We thank Cassandra Lamantia for assistance with animal management, John Olschowka and Kerry O'Banion for shared PCR resources, Fatima Rivera-Escalera for providing training on tissue preparation for microglial FACS, Anirvan Ghosh for the Sholl analysis ImageJ plugin, and Jianhua Cang for sharing Matlab code for OD analysis. This work was supported by the Nation Institutes of Health (NIH) grants R01 EY019277 (A.K.M), R21 NS099973 (A.K.M), R01 AA027111 (A.K.M), R01 EY028219 (M.S.), F31 NS105249 (R.D.S), T32 NS007489 (R.D.S, G.O.S), F31 NS086241 (G.O.S), F32 EY028028 (G.O.S), National Science Foundation grant NSF 1557971 (A.K.M), Schmitt Program on Integrative Brain Research grant (G.O.S, R.P.D), University of Rochester Bilski-Mayer Fellowship (H.N.B), and University of Rochester Medical Center Summer Scholars Fellowship (K.A.L.).

References

1. Schafer DP, Lehrman EK & Stevens B The "quad-partite" synapse: microglia-synapse interactions in the developing and mature CNS. Glia 61, 24–36, doi:10.1002/glia.22389 (2013). [PubMed: 22829357]
2. Nimmerjahn A, Kirchhoff F & Helmchen F Resting microglial cells are highly dynamic surveillants of brain parenchyma in vivo. Science 308, 1314–1318, doi:10.1126/science.1110647 (2005). [PubMed: 15831717]

3. Davalos D et al. ATP mediates rapid microglial response to local brain injury in vivo. Nat Neurosci 8, 752–758, doi:10.1038/nn1472 (2005). [PubMed: 15895084]
4. Tremblay ME, Lowery RL & Majewska AK Microglial interactions with synapses are modulated by visual experience. PLoS Biol 8, e1000527, doi:10.1371/journal.pbio.1000527 (2010). [PubMed: 21072242]
5. Miyamoto A et al. Microglia contact induces synapse formation in developing somatosensory cortex. Nat Commun 7, 12540, doi:10.1038/ncomms12540 (2016). [PubMed: 27558646]
6. Wake H, Moorhouse AJ, Jinno S, Kohsaka S & Nabekura J Resting microglia directly monitor the functional state of synapses in vivo and determine the fate of ischemic terminals. The Journal of neuroscience : the official journal of the Society for Neuroscience 29, 3974–3980, doi:10.1523/JNEUROSCI.4363-08.2009 (2009). [PubMed: 19339593]
7. Stowell RD et al. Cerebellar microglia are dynamically unique and survey Purkinje neurons in vivo. Dev Neurobiol 78, 627–644, doi:10.1002/dneu.22572 (2018). [PubMed: 29285893]
8. Schafer DP et al. Microglia sculpt postnatal neural circuits in an activity and complement-dependent manner. Neuron 74, 691–705, doi:10.1016/j.neuron.2012.03.026 (2012). [PubMed: 22632727]
9. Parkhurst CN et al. Microglia promote learning-dependent synapse formation through brain-derived neurotrophic factor. Cell 155, 1596–1609, doi:10.1016/j.cell.2013.11.030 (2013). [PubMed: 24360280]
10. Sipe GO et al. Microglial P2Y12 is necessary for synaptic plasticity in mouse visual cortex. Nat Commun 7, 10905, doi:10.1038/ncomms10905 (2016). [PubMed: 26948129]
11. Paolicelli RC et al. Synaptic pruning by microglia is necessary for normal brain development. Science 333, 1456–1458, doi:10.1126/science.1202529 (2011). [PubMed: 21778362]
12. Hoshiko M, Arnoux I, Avignone E, Yamamoto N & Audinat E Deficiency of the microglial receptor CX3CR1 impairs postnatal functional development of thalamocortical synapses in the barrel cortex. J Neurosci 32, 15106–15111, doi:10.1523/JNEUROSCI.1167-12.2012 (2012). [PubMed: 23100431]
13. Zhan Y et al. Deficient neuron-microglia signaling results in impaired functional brain connectivity and social behavior. Nat Neurosci 17, 400–406, doi:10.1038/nn.3641 (2014). [PubMed: 24487234]
14. Dissing-Olesen L et al. Activation of neuronal NMDA receptors triggers transient ATP-mediated microglial process outgrowth. J Neurosci 34, 10511–10527, doi:10.1523/JNEUROSCI.0405-14.2014 (2014). [PubMed: 25100586]
15. Ding F et al. alpha1-Adrenergic receptors mediate coordinated Ca2+ signaling of cortical astrocytes in awake, behaving mice. Cell Calcium 54, 387–394, doi:10.1016/j.ceca.2013.09.001 (2013). [PubMed: 24138901]
16. Xie L et al. Sleep drives metabolite clearance from the adult brain. Science 342, 373–377, doi:10.1126/science.1241224 (2013). [PubMed: 24136970]
17. Yang G et al. Sleep promotes branch-specific formation of dendritic spines after learning. Science 344, 1173–1178, doi:10.1126/science.1249098 (2014). [PubMed: 24904169]
18. Aton SJ et al. Mechanisms of sleep-dependent consolidation of cortical plasticity. Neuron 61, 454–466, doi:10.1016/j.neuron.2009.01.007 (2009). [PubMed: 19217381]
19. O'Donnell J, Zeppenfeld D, McConnell E, Pena S & Nedergaard M Norepinephrine: a neuromodulator that boosts the function of multiple cell types to optimize CNS performance. Neurochem Res 37, 2496–2512, doi:10.1007/s11064-012-0818-x (2012). [PubMed: 22717696]
20. Zhang Y et al. An RNA-sequencing transcriptome and splicing database of glia, neurons, and vascular cells of the cerebral cortex. J Neurosci 34, 11929–11947, doi:10.1523/JNEUROSCI.1860-14.2014 (2014). [PubMed: 25186741]
21. Nelson LE et al. The alpha2-adrenoceptor agonist dexmedetomidine converges on an endogenous sleep-promoting pathway to exert its sedative effects. Anesthesiology 98, 428–436 (2003). [PubMed: 12552203]
22. Bernier LP et al. Nanoscale Surveillance of the Brain by Microglia via cAMP-Regulated Filopodia. Cell Rep 27, 2895–2908 e2894, doi:10.1016/j.celrep.2019.05.010 (2019). [PubMed: 31167136]
23. Bellesi M, Tononi G, Cirelli C & Serra PA Region-Specific Dissociation between Cortical Noradrenaline Levels and the Sleep/Wake Cycle. Sleep 39, 143–154, doi:10.5665/sleep.5336 (2016). [PubMed: 26237776]

24. Gyoneva S & Traynelis SF Norepinephrine modulates the motility of resting and activated microglia via different adrenergic receptors. J Biol Chem 288, 15291–15302, doi:10.1074/jbc.M113.458901 (2013). [PubMed: 23548902]
25. Frenkel MY & Bear MF How monocular deprivation shifts ocular dominance in visual cortex of young mice. Neuron 44, 917–923 (2004). [PubMed: 15603735]
26. Gordon JA & Stryker MP Experience-dependent plasticity of binocular responses in the primary visual cortex of the mouse. J Neurosci 16, 3274–3286 (1996). [PubMed: 8627365]
27. Kasamatsu T & Pettigrew JD Depletion of brain catecholamines: failure of ocular dominance shift after monocular occlusion in kittens. Science 194, 206–209 (1976). [PubMed: 959850]
28. Pettigrew JD & Kasamatsu T Local perfusion of noradrenaline maintains visual cortical plasticity. Nature 271, 761–763 (1978). [PubMed: 625346]
29. Hinoi E et al. The sympathetic tone mediates leptin's inhibition of insulin secretion by modulating osteocalcin bioactivity. J Cell Biol 183, 1235–1242, doi:10.1083/jcb.200809113 (2008). [PubMed: 19103808]
30. Toth LA & Bhargava P Animal models of sleep disorders. Comp Med 63, 91–104 (2013). [PubMed: 23582416]
31. Wulff K, Gatti S, Wettstein JG & Foster RG Sleep and circadian rhythm disruption in psychiatric and neurodegenerative disease. Nat Rev Neurosci 11, 589–599, doi:10.1038/nrn2868 (2010). [PubMed: 20631712]
32. Polack PO, Friedman J & Golshani P Cellular mechanisms of brain state-dependent gain modulation in visual cortex. Nat Neurosci 16, 1331–1339, doi:10.1038/nn.3464 (2013). [PubMed: 23872595]
33. Frank MG, Issa NP & Stryker MP Sleep enhances plasticity in the developing visual cortex. Neuron 30, 275–287 (2001). [PubMed: 11343661]
34. Smith AJ, Yao X, Dix JA, Jin BJ & Verkman AS Test of the 'glymphatic' hypothesis demonstrates diffusive and aquaporin-4-independent solute transport in rodent brain parenchyma. Elife 6, doi:10.7554/eLife.27679 (2017).
35. Sipe GO et al. Microglial P2Y12 is necessary for synaptic plasticity in mouse visual cortex. Nature communications 7, doi:ARTN 1090510.1038/ncomms10905 (2016).
36. Schneble N et al. Phosphoinositide 3-kinase gamma ties chemoattractant- and adrenergic control of microglial motility. Mol Cell Neurosci 78, 1–8, doi:10.1016/j.mcn.2016.11.002 (2016). [PubMed: 27825984]
37. Madry C et al. Microglial Ramification, Surveillance, and Interleukin-1beta Release Are Regulated by the Two-Pore Domain K(+) Channel THIK-1. Neuron 97, 299–312 e296, doi:10.1016/j.neuron.2017.12.002 (2018). [PubMed: 29290552]
38. Madry C et al. Effects of the ecto-ATPase apyrase on microglial ramification and surveillance reflect cell depolarization, not ATP depletion. Proc Natl Acad Sci U S A 115, E1608–E1617, doi:10.1073/pnas.1715354115 (2018). [PubMed: 29382767]
39. Luo F & Zhou H Clenbuterol reduces GABAergic transmission in prefrontal cortex layer 5/6 pyramidal neurons of juvenile rat via reducing action potentials firing frequency of GABAergic interneurons. J Neurochem 144, 152–161, doi:10.1111/jnc.14248 (2018). [PubMed: 29086421]
40. Guneykaya D et al. Transcriptional and Translational Differences of Microglia from Male and Female Brains. Cell Rep 24, 2773–2783 e2776, doi:10.1016/j.celrep.2018.08.001 (2018). [PubMed: 30184509]
41. Smith JS & Rajagopal S The beta-Arrestins: Multifunctional Regulators of G Protein-coupled Receptors. J Biol Chem 291, 8969–8977, doi:10.1074/jbc.R115.713313 (2016). [PubMed: 26984408]
42. Li Y, Du X, Pei G, Du J & Zhao J beta-Arrestin1 regulates the morphology and dynamics of microglia in zebrafish in vivo. Eur J Neurosci 43, 131–138, doi:10.1111/ejn.13065 (2016). [PubMed: 26354363]
43. Qian L et al. beta2-adrenergic receptor activation prevents rodent dopaminergic neurotoxicity by inhibiting microglia via a novel signaling pathway. J Immunol 186, 4443–4454, doi:10.4049/jimmunol.1002449 (2011). [PubMed: 21335487]

44. Labrousse VF et al. Impaired interleukin-1beta and c-Fos expression in the hippocampus is associated with a spatial memory deficit in P2X(7) receptor-deficient mice. PLoS One 4, e6006, doi:10.1371/journal.pone.0006006 (2009). [PubMed: 19547756]
45. Kaneko M, Stellwagen D, Malenka RC & Stryker MP Tumor necrosis factor-alpha mediates one component of competitive, experience-dependent plasticity in developing visual cortex. Neuron 58, 673–680, doi:10.1016/j.neuron.2008.04.023 (2008). [PubMed: 18549780]
46. Krueger JM, Obal FJ, Fang J, Kubota T & Taishi P The role of cytokines in physiological sleep regulation. Ann N Y Acad Sci 933, 211–221 (2001). [PubMed: 12000022]
47. Kolmus K, Tavernier J & Gerlo S beta2-Adrenergic receptors in immunity and inflammation: stressing NF-kappaB. Brain Behav Immun 45, 297–310, doi:10.1016/j.bbi.2014.10.007 (2015). [PubMed: 25459102]
48. Lowery RL, Tremblay ME, Hopkins BE & Majewska AK The microglial fractalkine receptor is not required for activity-dependent plasticity in the mouse visual system. Glia 65, 1744–1761, doi: 10.1002/glia.23192 (2017). [PubMed: 28836393]
49. Madrigal JL, Caso JR, Garcia-Bueno B, Gutierrez IL & Leza JC Noradrenaline induces CX3CL1 production and release by neurons. Neuropharmacology 114, 146–155, doi:10.1016/j.neuropharm. 2016.12.001 (2017). [PubMed: 27923568]
50. Musiek ES & Holtzman DM Mechanisms linking circadian clocks, sleep, and neurodegeneration. Science 354, 1004–1008, doi:10.1126/science.aah4968 (2016). [PubMed: 27885006]
51. Jung S et al. Analysis of fractalkine receptor CX(3)CR1 function by targeted deletion and green fluorescent protein reporter gene insertion. Mol Cell Biol 20, 4106–4114 (2000). [PubMed: 10805752]
52. Feng G et al. Imaging neuronal subsets in transgenic mice expressing multiple spectral variants of GFP. Neuron 28, 41–51 (2000). [PubMed: 11086982]
53. Madisen L et al. A robust and high-throughput Cre reporting and characterization system for the whole mouse brain. Nat Neurosci 13, 133–140, doi:10.1038/nn.2467 (2010). [PubMed: 20023653]
54. Wong EL et al. Developmental alcohol exposure impairs synaptic plasticity without overtly altering microglial function in mouse visual cortex. Brain Behav Immun 67, 257–278, doi:10.1016/j.bbi. 2017.09.003 (2018). [PubMed: 28918081]
55. Ryan KM et al. Clenbuterol activates the central IL-1 system via the beta2-adrenoceptor without provoking inflammatory response related behaviours in rats. Brain Behav Immun 56, 114–129, doi:10.1016/j.bbi.2016.02.023 (2016). [PubMed: 26928198]
56. Frishman W Clinical pharmacology of the new beta-adrenergic blocking drugs. Part 9. Nadolol: a new long-acting beta-adrenoceptor blocking drug. Am Heart J 99, 124–128 (1980). [PubMed: 6101295]
57. Bilski AJ, Halliday SE, Fitzgerald JD & Wale JL The pharmacology of a beta 2-selective adrenoceptor antagonist (ICI 118,551). J Cardiovasc Pharmacol 5, 430–437 (1983). [PubMed: 6191142]
58. Jonsson G, Hallman H, Ponzio F & Ross S DSP4 (N-(2-chloroethyl)-N-ethyl-2-bromobenzylamine)--a useful denervation tool for central and peripheral noradrenaline neurons. Eur J Pharmacol 72, 173–188 (1981). [PubMed: 6265244]
59. Farneback G. Two-Frame Motion Estimation Based on Polynomial Expansion; Proceedings of the 13th Scandinavian Conference on Image Analysis; 2003.
60. Root DH et al. Norepinephrine activates dopamine D4 receptors in the rat lateral habenula. J Neurosci 35, 3460–3469, doi:10.1523/JNEUROSCI.4525-13.2015 (2015). [PubMed: 25716845]

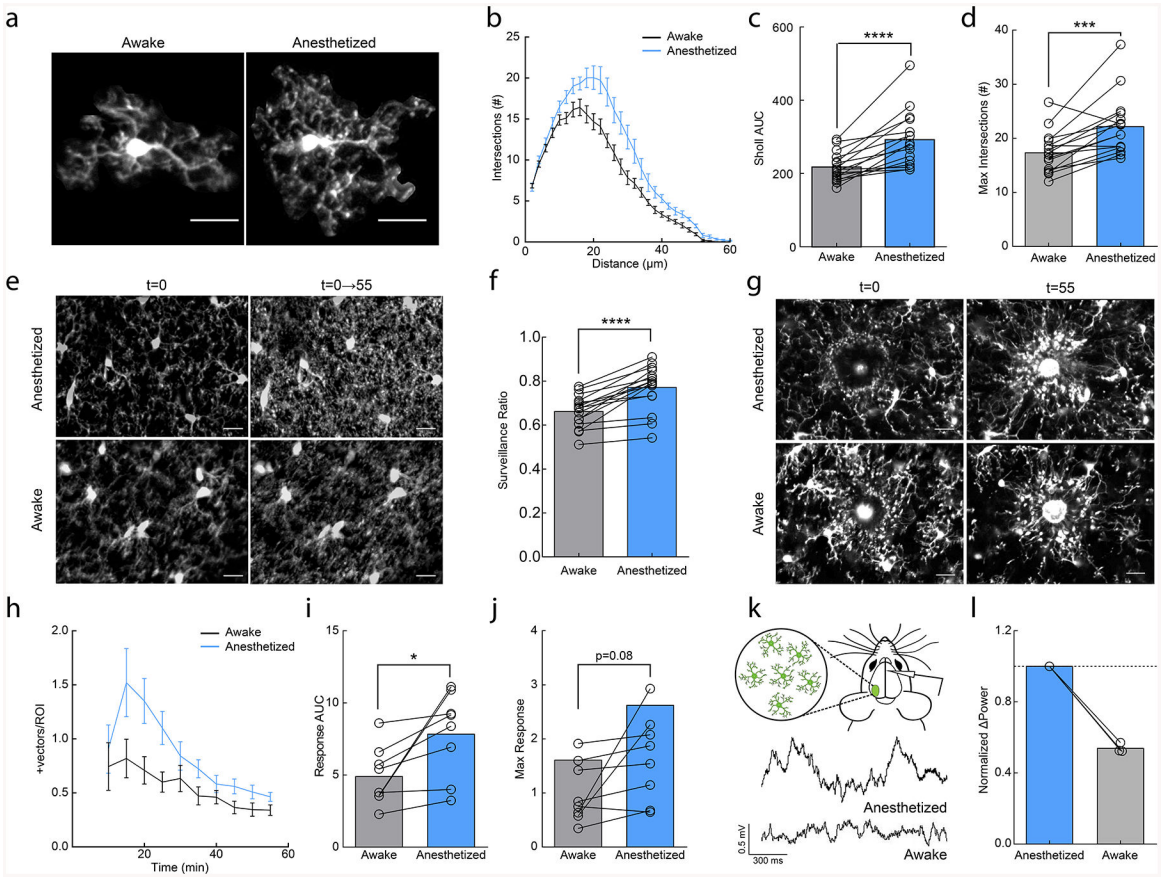

Figure 1|. Anesthesia enhances microglial surveillance of the parenchyma.

(**a**) Individual microglia from awake and anesthetized mice. (**b**) Sholl profile of microglia in awake (black and anesthetized (blue) mice; note reduced arborization in awake mice (n=16 mice, 3–5 microglia per mouse). (**c**) Microglia have a greater area under the curve (AUC) in anesthetized vs. awake mice (n=16 mice, two-sided paired t-test, $p=8.9\times10^{-5}$, t(15)=5.30). (**d**) Microglia have a greater number of maximum intersections in anesthetized mice (n=16 mice, two-sided paired t-test, p=0.00051, t(15)=4.40). (**e**) 2D max-projection of microglial processes at the first time point (t=0) and over one hour of imaging (t=0–55) to quantify process surveillance. (**f**) Microglia in anesthetized animals cover more of the CNS parenchyma (n=16 mice, two-sided paired t-test, $p=8.2\times10^{-6}$, t(15)=6.62). (**g**) Microglia in an awake or anesthetized mouse surrounding a focal laser ablation injury at t=0 and t=55 minutes post-ablation. (**h**) Graph of microglial process recruitment from 10 minutes post-injury to 55 minutes post-injury (velocity magnitude of responding vectors/total ROI pixels; n=8 mice). (**i**) Response AUC of microglial process recruitment from 10–55min post-injury (n=8 mice, two-sided paired t-test, P=0.025, t(7)=2.84). (**j**) Microglia trend towards a greater maximum magnitude of injury response in anesthetized conditions (n=8 mice, two-sided paired t-test, p=0.077, t(7)=2.08). (**k**) Example local field potential (LFP) traces in anesthetized and awake conditions. (**l**) Normalized delta-power from LFP recordings demonstrating decreased delta-power (~54%) in the awake state relative to the anesthetized state (n=3 mice). Scale bars = 20μm. Graphs show mean±SEM; *p<0.05, **p<0.01,

***p<0.005, ****p<0.0001. Points represent individual animals. See Supplementary Table 1 for the number of females and males used in these experiments.

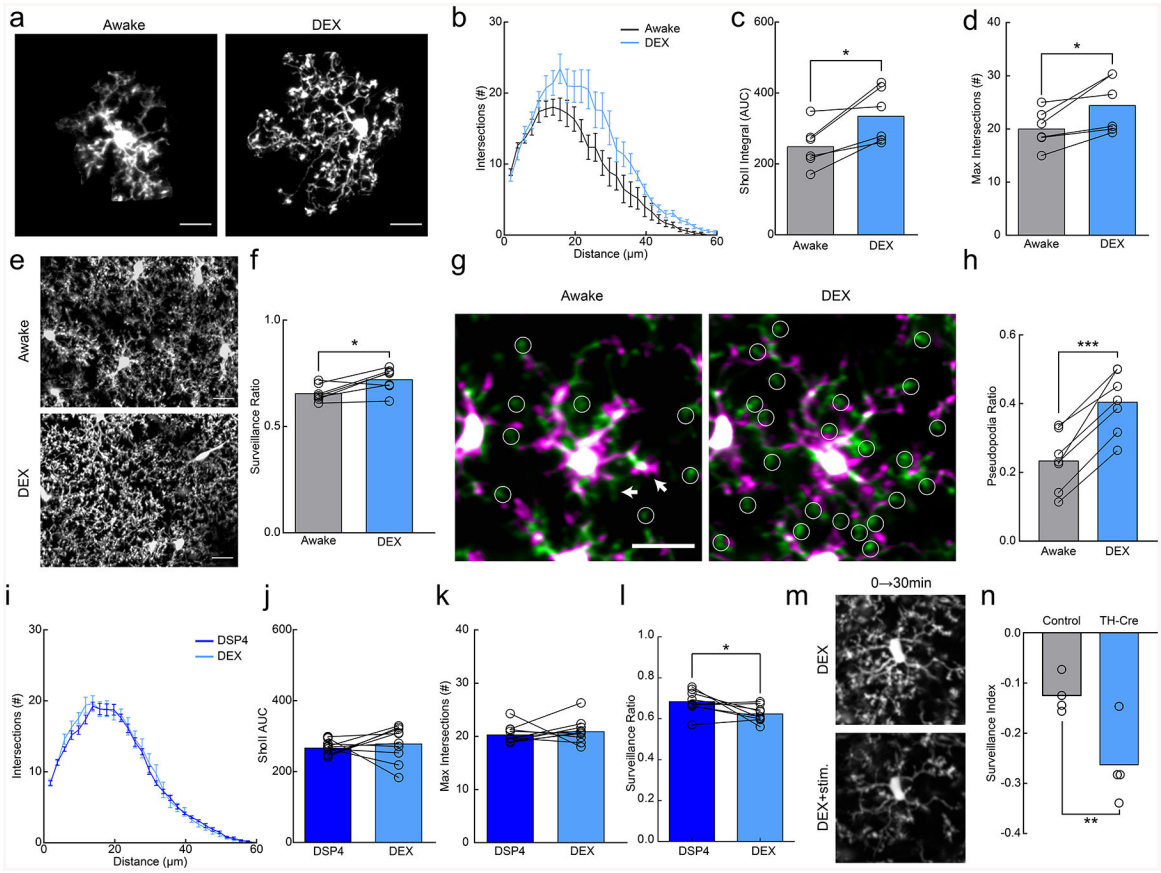

Figure 2|. Microglial surveillance is enhanced by dexmedetomidine.

(**a**) Example microglia in awake or dexmedetomidine-anesthetized (DEX) mice. (**b**) Sholl profile of microglia in awake (black) and DEX (blue); note increased ramification of microglial arbor with DEX (n=7 mice, 3–5 microglia per mouse). (**c**) Microglia in DEX-treated mice have a greater area under the curve (AUC) compared to those in awake mice (n=7 mice,, two-sided paired t-test, p=0.015, t(5)=3.63) and (**d**) a greater number of maximum process intersections (n=7 mice, two-sided paired t-test, p=0.024, t(6)=3.20). (**e**) 2D max-projection of microglial processes over an hour of imaging to quantify process surveillance. (**f**) Microglia in DEX-treated mice survey a greater portion of the CNS parenchyma (n=7 mice, two sided paired t-test, p=0.020, t(5)=3.13). (**g**) Overlays of two time points taken 10 minutes apart in awake and DEX-treated mice. Notice the increase in the extension (green) of pseudopodia (circles) after DEX. Arrows indicate filopodial extension (green) and retraction (magenta) in the awake state. (**h**) Quantification of the pseudopodia ratio showing a higher proportion of pseudopodia in DEX-treated animals (n=7 mice, two-sided paired t-test, p=0.00010, t(6)=9.01). (**i**) Sholl profile of DSP4-treated animals when awake (dark blue) and under DEX (light blue, n=10 mice, 3–5 microglia per mouse). (**j**) Sholl AUC shows no difference between awake and DEX-treatment in DSP4-treated mice (n=10 mice, two-sided paired t-test, p=0.55, t(9)=0.63). (**k**) There was also no significant difference in the maximum process intersections (n=10 mice, two-sided paired t-test, p=0.50, t(9)=0.69). (**l**) DSP4-treated mice had decreased surveillance ratio with DEX-treatment (n=9 mice, two-sided paired t-test, p=0.038, t(8)=2.48). (**m**) 2D max-projection of

microglial processes over 30 minutes in DEX-treated mice before and after optogenetic stimulation of locus coeruleus (LC) axons in the cortex. (**n**) Stimulation decreased the microglial surveillance index (laser stim surveillance - baseline surveillance/baseline surveillance) to a larger degree in TH-Cre+ than light-control CX3CR1$^{GFP/+}$ mice (n=4 mice, two-sided t-test, p=0.022, t(6)=3.08). Scale bars = 20μm. Graphs show mean±SEM; *p<0.05, **p<0.01, ***p<0.005. Points represent individual animals. See Supplementary Table 1 for the number of females and males used in these experiments.

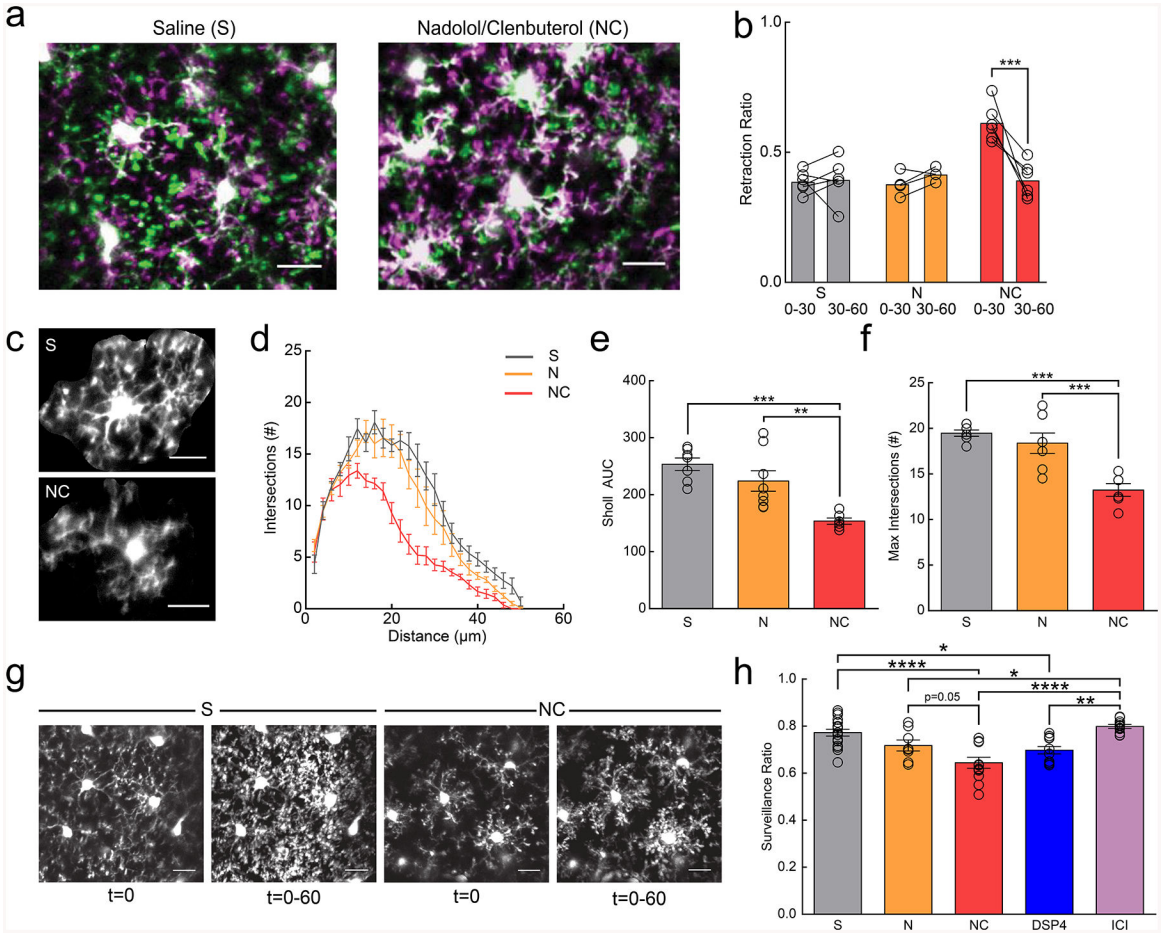

Figure 3|. β_2AR signaling reduces microglial dynamics in adolescent mice.

Anesthetized mice were imaged through a thin-skull preparation. (**a**) Overlay of microglia at t=0 (magenta) and t=30 (green) in mice treated with saline (S) or nadolol/clenbuterol (NC); note increased retraction of processes (magenta) in NC mice. (**b**) Microglia in mice treated with NC, but not S or nadolol only (N) have a rapid transient increase in the retraction ratio (retracted pseudopodia/total pseudopodia) from 0–30min (n: S=6, N=5, NC=6 mice, two-way RM-ANOVA, significant main effects of treatment (p=0.00084, F(2,13)=12.82) and time (p=0.0018, F(1,13)=15.27), and interaction (p=0.0026, F(2,13)=9.72). Holm-Sidak multiple comparisons, S v. NC, p=0.00011). (**c**) Example microglia from S and NC treated mice. (**d**) Sholl profile of S-, N-, and NC-treated mice; note the reduction in microglial arborization in NC-treated mice (n: S=7, N=8, NC=6 mice, 3–5 microglia per animal). (**e**) NC reduces Sholl area under the curve (AUC) (n: S=7, N=8, NC=6 mice, one-way ANOVA, p=0.00040, F(2,18)=12.45, Holm-Sidak multiple comparisons: S v. NC p=0.00036, N v. NC p=0.0045). (**f**) Maximum number of Sholl intersections is reduced in NC-treated microglia (n: S=7, N=8, NC=6 mice, one-way ANOVA, p=0.00019, F(2,18)=14.31, Holm-Sidak multiple comparisons: S v. NC p=0.00025, N v. NC p=0.00091). (**g**) Initial ramification (t=0) and 2D max-projections (t=0–60) of microglial process surveillance in S- and NC-treated mice; note decreased surveillance in the NC-treated mice. (**h**) Microglia in NC- and DSP4-treated mice survey less of the parenchyma (n: S=16, N=8, NC=12, DSP4=12, ICI=11

mice, one-way ANOVA, $p=2.6\times10^{-7}$, $F(4,55)=12.51$, Holm-Sidak multiple comparisons tests: S v. NC $p=6.6\times10^{-6}$, S v. DSP4 $p=0.013$, N v. ICI $p=0.034$, NC v. ICI $p=1.1\times10^{-6}$, DSP4 v. ICI $p=0.0015$). Scale bars = 20μm. Graphs show mean±SEM. Abbreviations: S=saline, N=nadolol, NC=nadolol/clenbuterol, DSP4=N-(2-Chloroethyl)-N-ethyl-2-bromobenzylamine, ICI=ICI-118,551; *p<0.05, **p<0.01, ***p<0.005, ****p<0.0001). Points represent individual animals. See Supplementary Table 1 for the number of females and males used in these experiments.

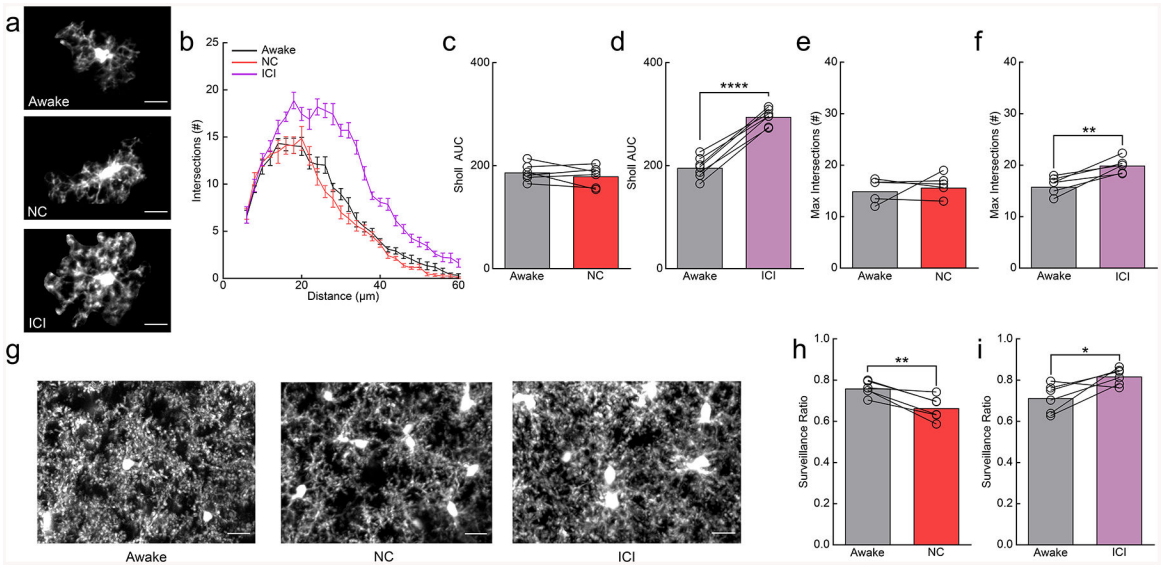

Figure 4|. Inhibition of β_2ARs in awake mice recapitulates the effects of anesthesia by enhancing microglial arborization and surveillance.

(**a**) Microglia from awake mice and nadolol/clenbuterol (NC) or ICI-118,551 (ICI) treated, awake mice. (**b**) Sholl profile of microglia in awake mice before (gray) and after NC (red) or ICI (purple) treatment (n: NC=6, ICI=7 mice, 3–5 microglia per animal); note the increase in microglial process arborization with ICI treatment. (**c**) The Sholl area under the curve (AUC) of awake mice given NC is not altered (n=6 mice, two-sided paired t-test, p=0.36, t(5)=1.00). (**d**) ICI-treatment increases the Sholl AUC in awake mice (n=7 mice, two-sided paired t-test, $p=5.8\times10^{-6}$, t(6)=14.89). (**e**) The maximum number of Sholl intersections is not altered with NC in awake mice (n=6 mice, two-sided paired t-test, p=0.60, t(5)=0.56). (**f**) The maximum number of Sholl intersections is increased by ICI in awake mice (n=7 mice, paired t-test, p=0.0019, t(6)=5.24). (**g**) 2D max-projections of microglial process surveillance from 0–60min; note decreased surveillance after NC and increased surveillance after ICI treatment. (**h**) Microglia in NC-treated, awake mice survey less of the parenchyma (n=6 mice, two-sided paired t-test, p=0.0045, t(5)=4.89). (**i**) Microglia in ICI-treated, awake mice have increased surveillance of the parenchyma (n=6 mice, two-sided paired t-test, p=0.029, t(5)=3.03). Scale bars = 20μm. Graphs show mean±SEM. Abbreviations: NC=nadolol/clenbuterol, ICI=ICI-118,551; *p<0.05, **p<0.01, ***p<0.005, ****p<0.0001). Points represent individual animals. See Supplementary Table 1 for the number of females and males used in these experiments.

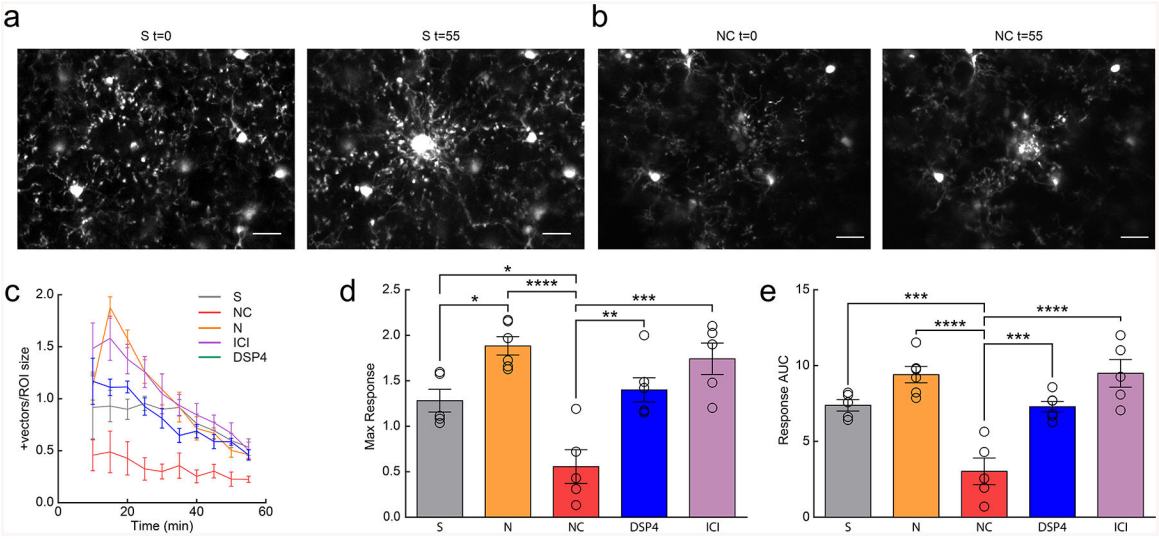

Figure 5|. β_2AR activation inhibits microglial process response to focal tissue injury.

(**a**) Example microglial response to focal laser ablation in a saline-treated (S) mouse at t=0 and t=55 minutes post-ablation. (**b**) Example microglial response to laser ablation in a nadolol/clenbuterol-treated (NC) mouse at t=0 and t=55 minutes post-ablation. (**c**) Microglial process response vectors from 10–55 minutes post-ablation (n: S=5, N=7, NC=5, DSP4=6, ICI=6 mice). (**d**) Microglia in NC-treated mice have a reduced maximum response to focal tissue injury (n: S=5, N=7, NC=5, DSP4=6, ICI=6 mice, one-way ANOVA, $p=1.7\times10^{-5}$, $F(4,26)=12.69$, Holm-Sidak multiple comparisons: S v. NC p=0.016, S v. N p=0.039, N v. NC $p=1.3\times10^{-5}$, NC v. DSP4 p=0.0031, and NC v. ICI p=0.00010). (**e**) Microglia in NC-treated mice have decreased response area under the curve (AUC) 10–55min post-ablation (n: S=5, N=7, NC=5, DSP4=6, ICI=6 mice, one-way ANOVA, $p=2.1\times10^{-6}$, $F(4,26)=16.65$, Holm-Sidak's multiple comparisons: S v. NC p=0.00073, N v. NC $p=3.1\times10^{-6}$, NC v. DSP4 p=0.00061, and NC v. ICI $p=4.5\times10^{-6}$). Scale bars = 20μm. Graphs show mean±SEM. Abbreviations: S=saline, N=nadolol, NC=nadolol/clenbuterol, ICI=ICI-118,551, DSP4=N-(2-Chloroethyl)-N-ethyl-2-bromobenzylamine; *p<0.05, **p<0.01, ***p<0.005, ****p<0.0001). Points represent individual animals. See Supplementary Table 1 for the number of females and males used in these experiments.

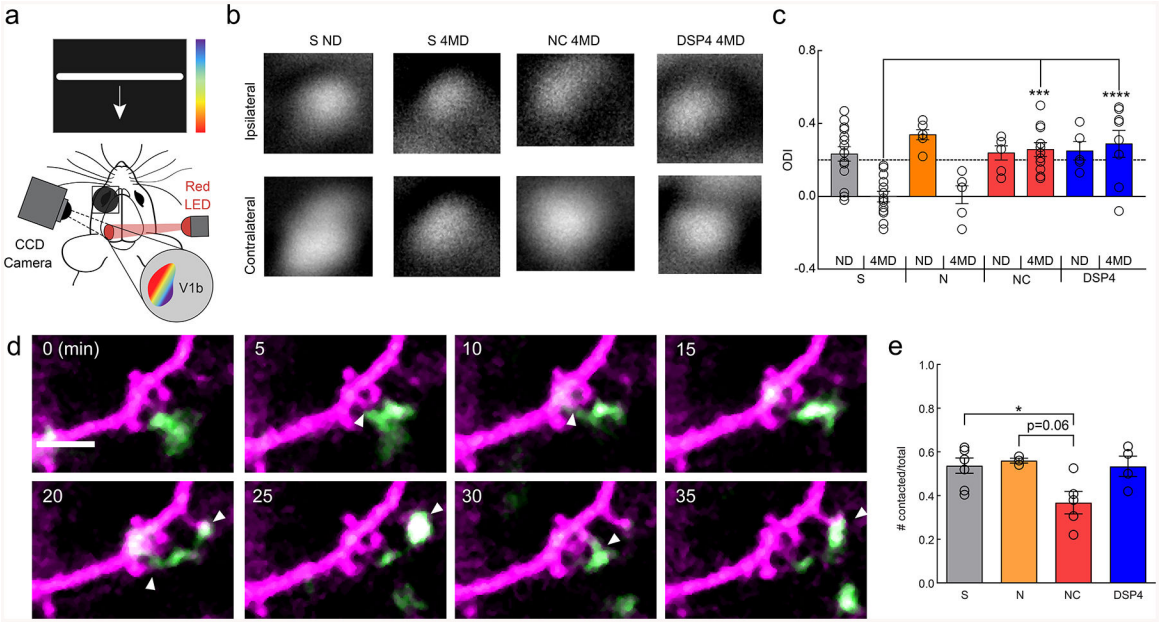

Figure 6|. Chronic microglial β_2AR activation impairs adolescent ocular dominance plasticity.
(**a**) Schematic of the intrinsic optical signal imaging. (**b**) Representative amplitude maps from stimulation of the ipsilateral (top) and contralateral (bottom) eyes for mice treated with saline (S), nadolol/clenbuterol (NC), and DSP4. Non-deprived (ND) maps are shown for S treatment. All other maps are after 4 days of monocular deprivation (4MD), these maps are representative of the presented findings. (**c**) Quantification of the ocular dominance index (ODI) demonstrates ocular dominance shifts with S and nadolol (N) treatment, but no shifts with NC and DSP4 treatment (n: S ND=15, S 4MD=14, N ND=6, N 4MD=6, NC ND=6, NC 4MD=11, DSP4 ND=6, DSP4 4MD=8 mice, two-way ANOVA, main effects of MD ($p=0.00033$, $F(1,76)=14.15$), and treatment ($p=0.0025$, $F(4,76)=4.51$), and interaction ($p=0.00035$, $F(4,76)=5.89$). Holm-Sidak multiple comparisons: S 4MD v. NC 4MD $p=0.00014$, S 4MD v. DSP4 4MD, $p=1.0\times10^{-5}$). (**d**) Example imaging of a single dendrite (magenta) and microglial process (green) across 35 minutes showing numerous putative microglia dendritic spine interactions (white arrowheads). (**e**) NC treatment reduces the proportion of dendritic spines contacted by microglial processes over one hour (n: S=7, N=3, NC=5, DSP4=4 mice, one-way ANOVA, $p=0.022$, $F(3,15)=4.35$, Holm-Sidak multiple comparisons: S v. NC $p=0.041$, N v. NC, $p=0.061$). Scale bar = 5μm. Graphs show mean ±SEM. Abbreviations: S=saline, N=nadolol, NC=nadolol/clenbuterol, ICI=ICI-118,551, DSP4= N-(2-Chloroethyl)-N-ethyl-2-bromobenzylamine; ND=non-deprived, 4MD=4 days monocular deprivation; *$p<0.05$, **$p<0.01$, ***$p<0.005$. Points represent individual animals. See Supplementary Table 1 for the number of females and males used in these experiments.

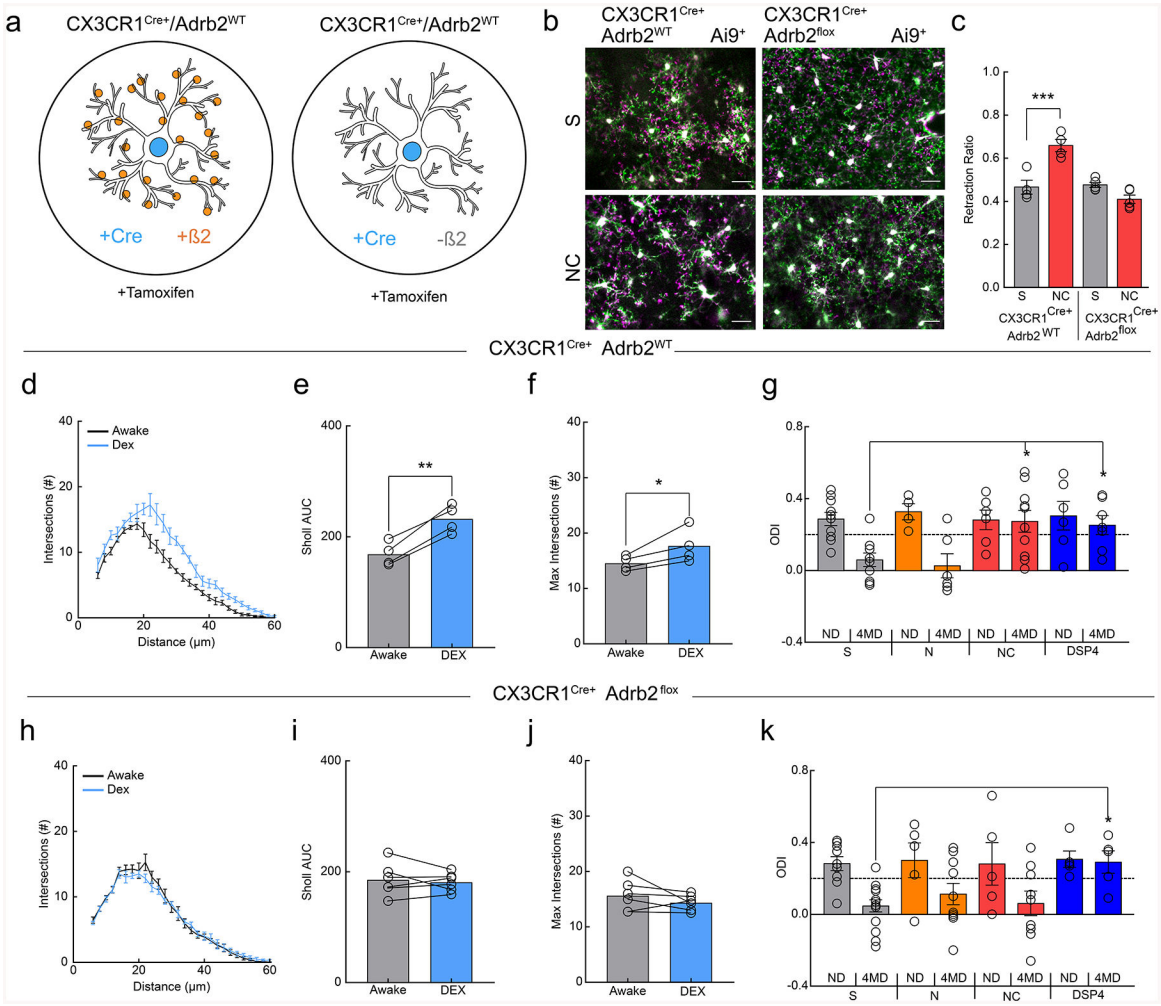

Figure 7|. Microglial β_2ARs mediate the effects of clenbuterol on ODP.

(**a**) Schematic of the transgenic lines used to generate microglia with and without β_2ARs (orange circles). (**b**) Example overlays of microglia at t=0 (magenta) and t=30 (green) in CX3CR1-Cre/Ai9 and CX3CR1-Cre/B2/Ai9 mice after treatment with saline (S) or nadolol/clenbuterol (NC). Note the absence of increased retraction (magenta) after NC in microglia lacking β_2ARs. (**c**) Ablation of microglial β_2ARs prevents NC-induced pseudopodia retraction (n: CreAi9 S=4, CreAi9 NC=4, CreB2Ai9 S=5, CreB2Ai9 NC=5 mice, two-way, RM-ANOVA, significant main effects of genotype (p=0.00083, F(1,7)=31.22) and treatment (p=0.035, F(1,7)=6.77), and interaction (p=0.0011, F(1,7)=28.56). Holm-Sidak multiple comparisons, CreAi9S v. CreAi9NC p=0.0022). (**d**) Sholl profile of awake (black) and dexmedetomidine-treated (DEX; blue), CX3CR1-Cre/Ai9 mice (n=4 mice, 3–5 microglia per mouse). DEX treatment increases the (**e**) Sholl area under the curve (AUC, n=4 mice, two-sided paired t-test, p=0.0033, t(3)=8.61) and the (**f**) maximum Sholl intersections (n=4 mice, two-sided paired t-test, p=0.047, t(3)=3.27). (**g**) Quantification of the ocular dominance index (ODI) in CX3CR1-Cre mice demonstrates robust ocular dominance shifts in mice with S and nadolol (N) treatment, but no shifts in mice with NC and DSP4 treatment (n: S ND=10, S 4MD=9, N ND=4, N 4MD=5, NC ND=6, NC 4MD=10, DSP4 ND=6, DSP4

4MD=7 mice, two-way ANOVA, significant main effect of monocular deprivation (p=0.00067, F(1,51)=13.12), and interaction (p=0.045, F(3,51)=2.88), Holm-Sidak multiple comparisons: S 4MD, v. NC 4MD p=0.0067, S 4MD v. DSP4 4MD p=0.022). (**h**) Sholl profiles of awake (black) and DEX-treated (blue) CX3CR1-Cre/B2/Ai9 mice show similar microglial process arborization (n=6 mice, 3–5 microglia per mouse) with no changes in (**i**) Sholl AUC (n=6 mice, two-sided paired t-test, p=0.63, t(5)=0.51) or the (**j**) maximum Sholl intersections (n=6 mice, two-sided paired t-test, p=0.27, t(5)=1.23). (**k**) Quantification of ODI in CX3CR1-Cre/B2 mice. Ablation of microglial β_2ARs rescues plasticity in NC-treated mice, but not DSP4-treated mice (n: S ND=9, S 4MD=15, N ND=5, N 4MD=9, NC ND=5, NC 4MD=9, DSP4 ND=5, & DSP4 4MD=5 mice, two-way ANOVA, main effect of MD (p=0.00080, F(1,54)=12.62). Holm-Sidak multiple comparisons: S 4MD, v. DSP4 4MD, p=0.046). Scale bar = 20μm. Graphs show mean±SEM. Abbreviations: S=saline, N=nadolol, NC=nadolol/clenbuterol, DSP4=N-(2-Chloroethyl)-N-ethyl-2-bromobenzylamine, DEX=dexmedetomidine; ND=non-deprived, 4MD=4 days monocular deprivation; *p<0.05, **p<0.01, ***p<0.005. Points represent individual animals. See Supplementary Table 1 for the number of females and males used in these experiments.